Part III

The Multi-Wavelength Properties of Gamma-Ray Burst Host Galaxies

CHAPTER 9

The Faint Optical Afterglow and Host Galaxy of GRB 020124: Implications for the Nature of Dark Gamma-Ray Bursts†

E. Berger[a], S. R. Kulkarni[a], J. S. Bloom[a], P. A. Price[a,b], D. W. Fox[a], D. A. Frail[a,c], T. S. Axelrod[b], R. A. Chevalier[d], E. Colbert[e], E. Costa[f], S. G. Djorgovski[a], F. Frontera[g,h], T. J. Galama[a], J. P. Halpern[i], F. A. Harrison[a], J. Holtzman[j], K. Hurley[k], R. A. Kimble[l], P. J. McCarthy[m], L. Piro[f], D. Reichart[a], G. R. Ricker[n], R. Sari[o], B. P. Schmidt[b], J. C. Wheeler[p], R. Vanderspek[n], & S. A. Yost[a]

[a]Department of Astronomy, 105-24 California Institute of Technology, Pasadena, CA 91125, USA

[b]Research School of Astronomy & Astrophysics, Mount Stromlo Observatory, via Cotter Rd., Weston Creek 2611, Australia

[c]National Radio Astronomy Observatory, Socorro, NM 87801

[d]Department of Astronomy, University of Virginia, P.O. Box 3818, Charlottesville, VA 22903-0818

[e]Department of Physics and Astronomy, Johns Hopkins University, 3400 N. Charles St., Baltimore, MD 21218

[f]Istituto Astrofisica Spaziale, C.N.R., Area di Tor Vergata, Via Fosso del Cavaliere 100, 00133 Roma, Italy

[g]Istituto Astrofisica Spaziale and Fisica Cosmica, C.N.R., Via Gobetti, 101, 40129 Bologna, Italy

[h]Physics Department, University of Ferrara, Via Paradiso, 12, 44100 Ferrara, Italy

[i]Columbia Astrophysics Laboratory, Columbia University, 550 West 120th Street, New York, NY 10027

[j]Department of Astronomy, MSC 4500, New Mexico State University, P.O. Box 30001, Las Cruces, NM 88003

[k]University of California at Berkeley, Space Sciences Laboratory, Berkeley, CA 94720-7450

[l]Laboratory for Astronomy and Solar Physics, NASA Goddard Space Flight Center, Code 681, Greenbelt, MD 20771

[m]Carnegie Observatories, 813 Santa Barbara Street, Pasadena, CA 91101

[n]Center for Space Research, Massachusetts Institute of Technology, 70 Vassar Street, Cambridge, MA 02139-4307

[o]Theoretical Astrophysics 130-33, California Institute of Technology, Pasadena, CA 91125

[p]Astronomy Department, University of Texas, Austin, TX 78712

† A version of this chapter was published in *The Astrophysical Journal*, vol. 590, 379–385, (2003).

Abstract

We present ground-based optical observations of GRB 020124 starting 1.6 hours after the burst, as well as subsequent Very Large Array (VLA) and *Hubble Space Telescope* (HST) observations. The optical afterglow of GRB 020124 is one of the faintest afterglows detected to date, and it exhibits a relatively rapid decay, $F_\nu \propto t^{-1.60\pm0.04}$, followed by further steepening. In addition, a weak radio source was found coincident with the optical afterglow. The HST observations reveal that a positionally coincident host galaxy must be the faintest host to date, $R \gtrsim 29.5$ mag. The afterglow observations can be explained by several models requiring little or no extinction within the host galaxy, $A_V^{\rm host} \approx 0 - 0.9$ mag. These observations have significant implications for the interpretation of the so-called dark bursts (bursts for which no optical afterglow is detected), which are usually attributed to dust extinction within the host galaxy. The faintness and relatively rapid decay of the afterglow of GRB 020124, combined with the low inferred extinction indicate that some dark bursts are intrinsically dim and not dust obscured. Thus, the diversity in the underlying properties of optical afterglows must be observationally determined before substantive inferences can be drawn from the statistics of dark bursts.

SECTION 9.1

Introduction

One of the main observational results stemming from five years of γ-ray burst (GRB) follow-ups at optical wavelengths is that about 60% of well-localized GRBs lack a detected optical afterglow, ("dark bursts"; Taylor et al. 2000; Fynbo et al. 2001; Lazzati et al. 2002; Reichart & Yost 2001. In some cases, a non-detection of the optical afterglow could simply be due to a failure to image quickly and/or deeply enough. However, there are two GRBs for which there is strong evidence that the optical emission should have been detected, based on an extrapolation of the radio and X-ray emission (Djorgovski et al. 2001a; Piro et al. 2002). One interpretation in these two cases is that the optical light was extinguished by dust, either within the immediate environment of the burst or elsewhere along the line of sight (e.g., Groot et al. 1998. An alternative explanation is a high redshift, leading to absorption of the optical light in the Lyα forest. However, the redshifts of the underlying host galaxies of these GRBs are of order unity (Djorgovski et al. 2001a; Piro et al. 2002).

Several authors have recently argued that a large fraction of the dark bursts are due to dust extinction within the local environment of the bursts (e.g., Lazzati et al. 2002; Reichart & Price 2002; Reichart & Yost 2001), but other scenarios have also been suggested (e.g., Lazzati et al. 2002). Moreover, it has been noted that regardless of the location of extinction within the host galaxy, the fraction of dark bursts is a useful upper limit on the fraction of obscured star formation (Kulkarni et al. 2000; Djorgovski et al. 2001b; Ramirez-Ruiz et al. 2002; Reichart & Price 2002).

However, from an observational point of view, we must have a clear understanding of the diversity of afterglow properties before extracting astrophysically interesting inferences from dark bursts. For example, afterglows which are intrinsically faint or fade rapidly (relative to the detected population) would certainly bias the determination of the fraction of truly obscured bursts. In this vein, Fynbo et al. (2001), noting the faint optical afterglow of GRB 000630, argue that some dark bursts are due to a failure to image deeply and/or quickly enough, rather than dust extinction. Observations of the faint afterglow of GRB 980613 (Hjorth et al. 2002) point to the same conclusion.

Here we present optical and radio observations of GRB 020124, an afterglow that would have been classified dark had it not been for rapid and deep searches. Furthermore, GRB 020124 is an example of an afterglow, which is dim due to the combination of intrinsic faintness and a relatively fast decline, and not strong extinction.

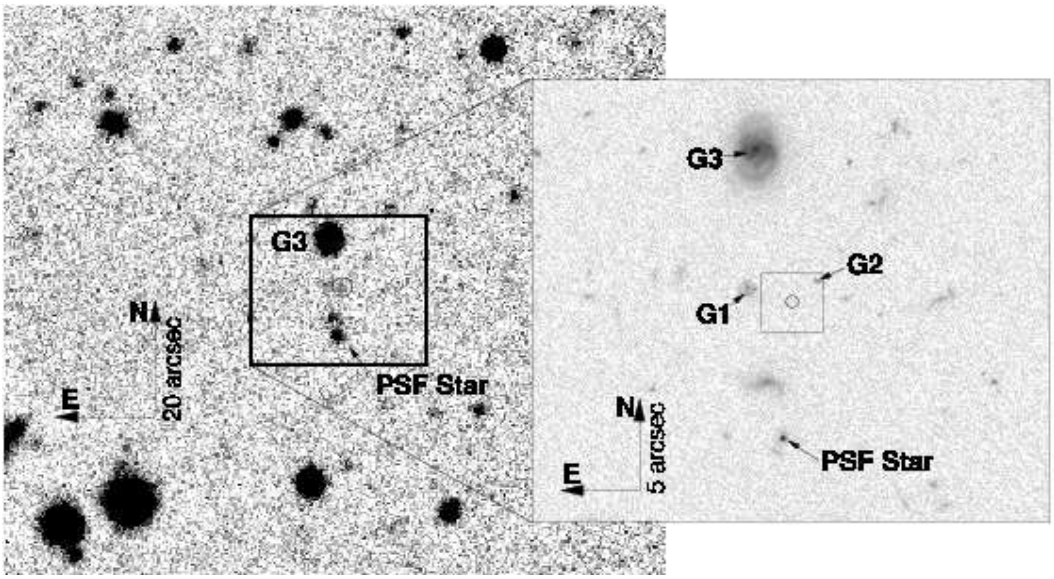

Figure 9.1: Palomar 200-inch (left) and HST epoch 1 (inset) images of the field of GRB 020124. The OT is circled in both images. The OT was of comparable brightness to G1 at the epoch of the P 200 image and significantly fainter than G1 three weeks later. The box overlaying the inset shows the portion of the HST images depicted in Figure 9.2. Relevant sources described in the text are noted. The HST image is shown with logarithmic scaling to highlight the features of nearby galaxies.

SECTION 9.2

Observations

9.2.1 Ground-Based Observations

GRB 020124, localized by the HETE-II satellite on 2002, Jan 24.44531 UT, had a duration of ~ 70 s and a fluence ($6 - 400$ keV) of 3×10^{-6} erg cm^{-2} (Ricker et al. 2002). Eight minutes after receiving the coordinates[1] we observed the error box with the dual-band (B_M, R_M) MACHO imager mounted on the robotic 50-in telescope at the Mount Stromlo Observatory (MSO). We also observed the error box with the Wide-Field Imager on the 40-in telescope at Siding Spring Observatory (SSO). We were unable to identify a transient source within the large error box (Price et al. 2002c).

We subsequently observed the error box refined by the Inter-Planetary Network (Hurley et al. 2002) with the Palomar 48-in Oschin Schmidt using the unfiltered NEAT imager. PSF-matched image subtraction (Alard 2000) between the MACHO and NEAT images revealed a fading source (Price et al. 2002b), which was $R \approx 18$ mag at the epoch of our first observations, and not present in the Digitized Sky Survey. Two nights later we observed the afterglow using the Jacobs CAMera (JCAM) mounted at the East arm focus of the Palomar 200-in telescope (Bloom 2002). The position of the fading source is α(J2000)=$9^{\rm h}32^{\rm m}50.78^{\rm s}$, δ(J2000)=$-11^\circ 31' 10.6''$, with an uncertainty of about 0.4 arcsec in each coordinate (Figure 9.1).

Using the Very Large Array (VLA[2]) we observed the fading source at 8.46 and 22.5 GHz (see Table 9.3). We detect a faint source, possibly fading, at 8.46 GHz located at α(J2000)=$9^{\rm h}32^{\rm m}50.81^{\rm s}$, δ(J2000)= $-11^\circ 31' 10.6''$, with an uncertainty of about 0.1 arcsec in each coordinate. Given the positional coincidence between the fading optical source and radio detection we suggest this source to be the afterglow of GRB 020124.

The optical images were bias-subtracted and flat-fielded in the standard manner. To extract the

[1] This corresponds to 1.6 hours after the burst detection.

[2] The VLA is operated by the National Radio Astronomy Observatory, a facility of the National Science Foundation operated under cooperative agreement by Associated Universities, Inc.

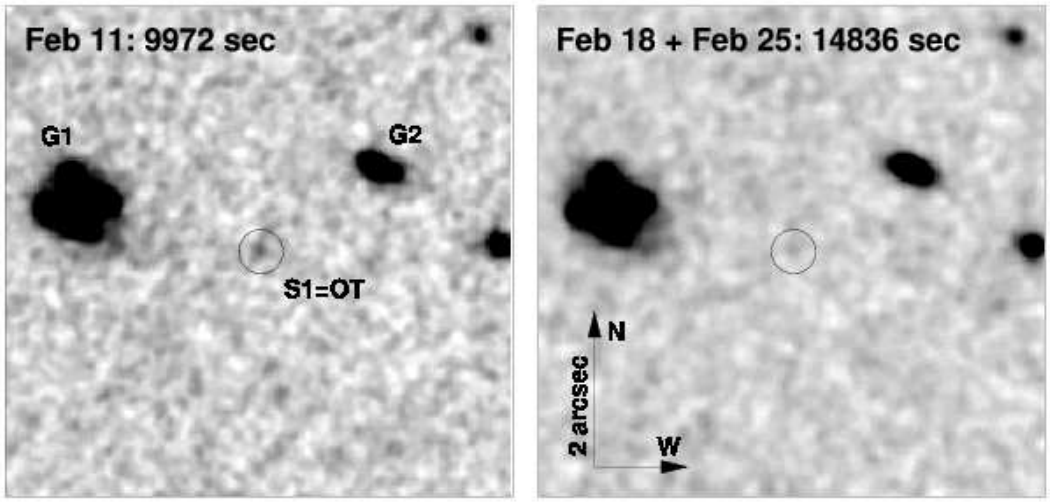

Figure 9.2: The faint optical transient (OT) of GRB 020124 as viewed using HST/STIS. Shown are the summed, smoothed images from epoch 1 (left) and epochs 2+3 (right). The grey-scales have been matched such that a given flux is represented by the same shade in each image. The circle is centered at the same sky position in both images. Clearly, the source S1, identified with the position of the afterglow of GRB 020124 has faded.

photometry we weighted the aperture with a Gaussian equivalent to the seeing disk ("weighted-aperture photometry"), using IRAF/`wphot`. The photometric zero-points were set through photometry of calibrated field stars (Henden 2002) with magnitudes transformed to the appropriate system (Bessell & Germany 1999; Smith et al. 2002b). The photometry is summarized in Table 9.1.

9.2.2 *Hubble Space Telescope* Observations

We observed the afterglow with the *Hubble Space Telescope* (HST) using the Space Telescope Imaging Spectrograph (STIS) on 2002 Feb. 11.09, 18.30, and 25.71 UT Bloom et al. (2002c), as part of our HST Cycle 10 program (GO-9180, PI: Kulkarni). The HST observations consisted of 750–850 sec exposures. The HST data were retrieved after "On-The-Fly" pre-processing. Using IRAF we drizzled (Fruchter & Hook 2002) each image onto a grid with pixels smaller than the original by a factor of two and using `pixfrac` of 0.7.

We found an astrometric tie between the HST and JCAM images using IRAF/`geomap` with nine suitable astrometric tie objects in common between the images. The rms of the resultant mapping is 133 mas (RA) and 124 mas (Dec). Using this mapping and IRAF/`geoxytrans` we transfered the afterglow position on the JCAM image to the HST images. The rms of the transformation is 604 mas (RA) and 596 mas (Dec), and is dominated by the uncertainty in the JCAM position.

The source "S1" (Figure 9.2) coincides with the afterglow position within the astrometric uncertainty. We performed differential photometry at the position of S1 by registering the images of epochs 1 and 2 using a cross-correlation of a field of size 10 arcsec centered on S1 (using IRAF/`crosscor` and `shiftfind`). We used IRAF/`center` and the FWHM of a relatively bright point source ("PSF star"; Figure 9.1) to fix the position of S1 in each of the final images, and to determine the uncertainty in the position.

We photometered the source (and the PSF star) in epoch 1 using IRAF/`phot`, in a 3.4 pix (86 mas) drizzled aperature radius. The small radius was chosen to maximize the signal-to-noise of the detection of the faint point source although, as found using the STIS instrument manual and confirmed with the PSF star, this radius encircles only $\sim 55\%$ of the light of a point source. A corresponding correction was applied to the fluxes found in this aperature; we estimate a 0.1 mag sytematic uncertainty due to

this correction. Using IRAF/`synphot`, and assuming a source spectrum of $f_\lambda \propto \lambda^{-0.5}$ (see below), we find that the source was $R = 28.68^{-0.20}_{+0.25}$ mag at the time of epoch 1. A bluer spectrum would result in an even fainter R-band magnitude, by as much as 0.25 mag for $f_\lambda \propto \lambda^{-2.5}$. More importantly, a redder spectrum would have little effect at R-band, with an increase of < 0.05 mag. The photometry of the three epochs is summarized in Table 9.2. Note that this more careful analysis supersedes our preliminary report (Bloom et al. 2002c).

There are no obvious persistent sources within 1.75 arcsec of the OT down to $R \approx 29.5$ mag. To date, all of the GRBs localized to sub-arcsecond accuracy have viable hosts brighter than this level within ~ 1.3 arcsec of the OT position (Bloom et al. 2002a). The faintest host to date is that of GRB 990510, $R \sim 28.5$ mag (z=1.619; Vreeswijk et al. 2001b). Thus, the host of GRB 020124 may be at a somewhat higher redshift; however, $z \lesssim 4.5$ since the afterglow was detected in the B_M filter.

SECTION 9.3

Modeling of the Optical Data

In Figure 9.3 we plot the optical light curves of GRB 020124, including a correction for Galactic extinction, $E(B-V) = 0.052$ mag (Schlegel et al. 1998). The optical light curves are usually modeled as $F_\nu(t,\nu) = F_{\nu,0}(t/t_0)^\alpha(\nu/\nu_0)^\beta$. However, as can be seen in Figure 9.3, the R-band light curve cannot be described by a single power law. Restricting the fit to $t < 2$ days we obtain ($\chi^2_{\rm min} = 15$ for 14 degrees of freedom) $\alpha_1 = -1.60 \pm 0.04$, $\beta = -1.43 \pm 0.14$, and $F_{\nu,0} = 2.96 \pm 0.25$ μJy; here $F_{\nu,0}$ is defined at the effective frequency of the R_M filter and $t = 1$ day. For $t > 2$ days we get $\alpha_2 = -1.9^{+1.0}_{-2.0}$. The uncertainty in α_2 is large because it is effectively constrained by only two data points. However, if we make the additional requirement that the fits to the ground-based data and the HST data intersect at $t > 2$ days, we find that $\alpha_2 = -1.9^{+0.1}_{-2.0}$, and the steepening is therefore significant at the 2.5σ level.

To account for the steepening we modify the model for the R-band light curve to:

$$F_\nu(t,\nu) = F_{\nu,0}(\nu/\nu_0)^\beta[(t/t_b)^{\alpha_1 n} + (t/t_b)^{\alpha_2 n}]^{1/n}, \quad (9.1)$$

where, α_1 is the asymptotic index for $t \ll t_b$, α_2 is the asymptotic index for $t \gg t_b$, $n < 0$ provides a smooth joining of the two asymptotic segments, and t_b is the time at which the asymptotic segments intersect. We retain the simple model for the R_M and B_M light curves since they are restricted to $t \lesssim 0.13$ days (i.e., well before the observed steepening).

We investigate two alternatives for the observed steepening in the framework of the afterglow synchrotron model (e.g., Sari et al. 1998), namely (i) a cooling break (§9.3.1), and (ii) a jet break (§9.3.2). In this framework, α_1, α_2, and β are related to each other through the index (p) of the electron energy distribution, $N(\gamma) \propto \gamma^{-p}$ (for $\gamma > \gamma_{\rm min}$). The relations for the models discussed below, as well as the resulting closure relations, $\alpha_1 + b\beta + c = 0$, are summarized in Table 9.4.

9.3.1 Cooling Break

The observed steepening, $\Delta\alpha \equiv \alpha_2 - \alpha_1 \approx -0.3$, can be due to the passage of the synchrotron cooling frequency, ν_c, through the R-band[3] . This has been suggested, for example, in the afterglow of GRB 971214, at $t \sim 0.6$ days (Wijers & Galama 1999). If the steepening is due to ν_c, this rules out models in which the ejecta expand into a circumburst medium with $\rho \propto r^{-2}$ (hereafter, Wind), because in this model ν_c increases with time ($\propto t^{1/2}$; Chevalier & Li 1999), and one expects $\Delta\alpha = 0.25$.

There are two remaining models to consider in this case: (i) spherical expansion into a circumburst medium with constant density (hereafter, ISM$_{\rm B}$; Sari et al. 1998), and (ii) a jet with $\theta_{\rm jet} < \Gamma^{-1}_{t\sim 0.06\,{\rm d}}$ (i.e.,

[3] We note that while the passage of ν_c through the R-band will also change the spectrum of the afterglow by $\delta\beta = -0.5$ (i.e., the afterglow would become somewhat redder), this has little effect on the conversion of the STIS count-rate to R-band magnitudes (see §9.2.2). We therefore use the same source magnitudes listed in Table 9.2, along with the relevant systematic uncertainties.

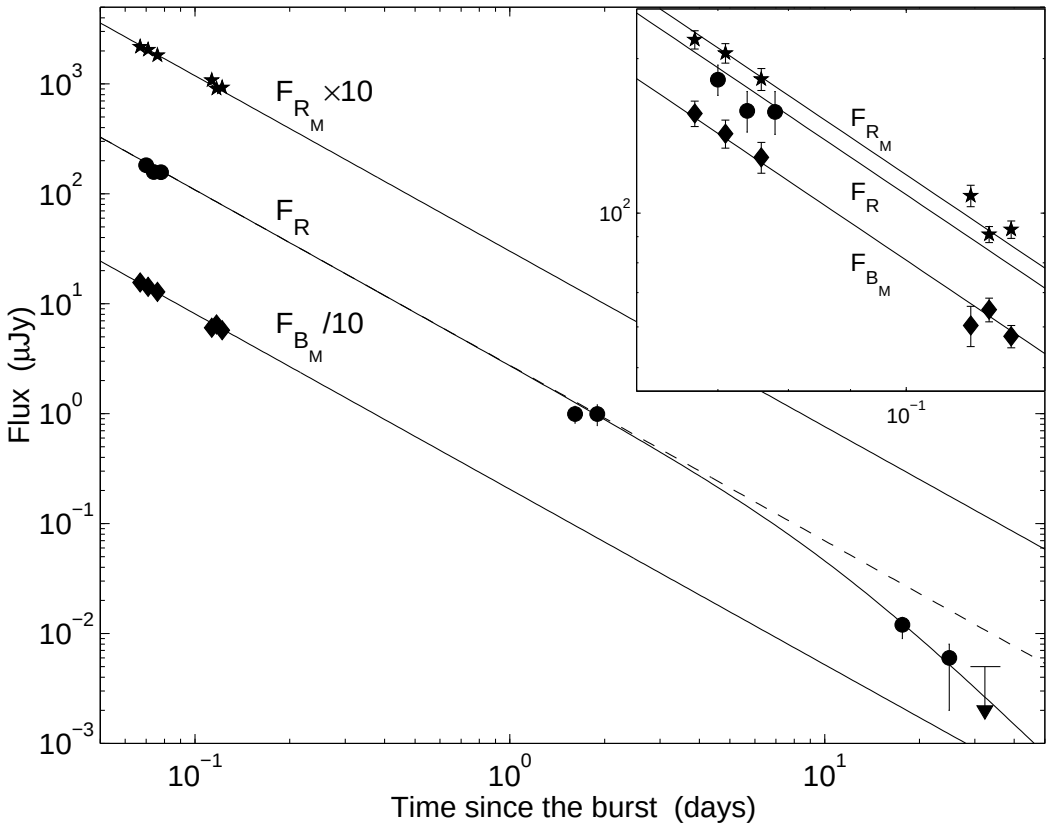

Figure 9.3: Optical light curves of GRB 020124 (top to bottom: R_M, R, and B_M), corrected for Galactic extinction, $E(B-V) = 0.052$ mag (Schlegel et al. 1998). The solid lines are a representative jet model (ISM/Wind$_{\rm R}$; see Table 9.4), while the dashed line is an extrapolation of the early evolution without a break. With no break in the R-band light curve, the predicted magnitude at the epoch of the first HST observation exceeds the measured values by 5σ. The flux measured in the last HST epoch is plotted as a 2σ upper limit.

a jet break prior to the first observation at $t \approx 0.06$ days; hereafter, Jet$_{\rm B}$). The subscript B indicates that ν_c is blueward of the optical bands initially. In both models we use Eqn. 9.1 for the R-band light curve, with t_b defined as the time at which $\nu_c = \nu_R$, and $\alpha_2 \equiv \alpha_1 - 1/4$.

We find that in the ISM$_{\rm B}$ model $t_c \approx 0.4$ days, while in the Jet$_{\rm B}$ model $t_c \approx 0.65$ days. Moreover, in both models the closure relations can only be satisfied by including a contribution from dust extinction within the host galaxy, $A_V^{\rm host}$. We estimate the required extinction using the parametric extinction curves of Cardelli et al. (1989) and Fitzpatrick & Massa (1988), along with the interpolation calculated by Reichart (2001). Since the redshift of GRB 020124 is not known we assume $z = 0.3$, 1, 3, which spans the range of typical redshifts for the long-duration GRBs. The inferred values of $A_V^{\rm host}$ are summarized in Table 9.4, and range from 0.2 to 0.9 mag.

9.3.2 Jet Break

An alternative explanation for the steepening is a jet expanding into: (i) an ISM medium with ν_c blueward of the optical bands (J-ISM$_{\rm B}$), (ii) a Wind medium with ν_c blueward of the optical bands (J-Wind$_{\rm B}$), and (iii) an ISM or Wind medium with ν_c redward of the optical bands (J-ISM/Wind$_{\rm R}$). We note that the J-ISM$_{\rm B}$ model is different than the ISM$_{\rm B}$ model (§9.3.1) since previously it was implicitly defined such that the jet break is later than the last observation. In these models, $t_b \equiv t_{\rm jet}$ is the time at which $\Gamma(t_{\rm jet}) \approx \theta_{\rm jet}^{-1}$.

From the closure values we note that the J-ISM/Wind$_{\rm R}$ requires no extinction within the host galaxy,

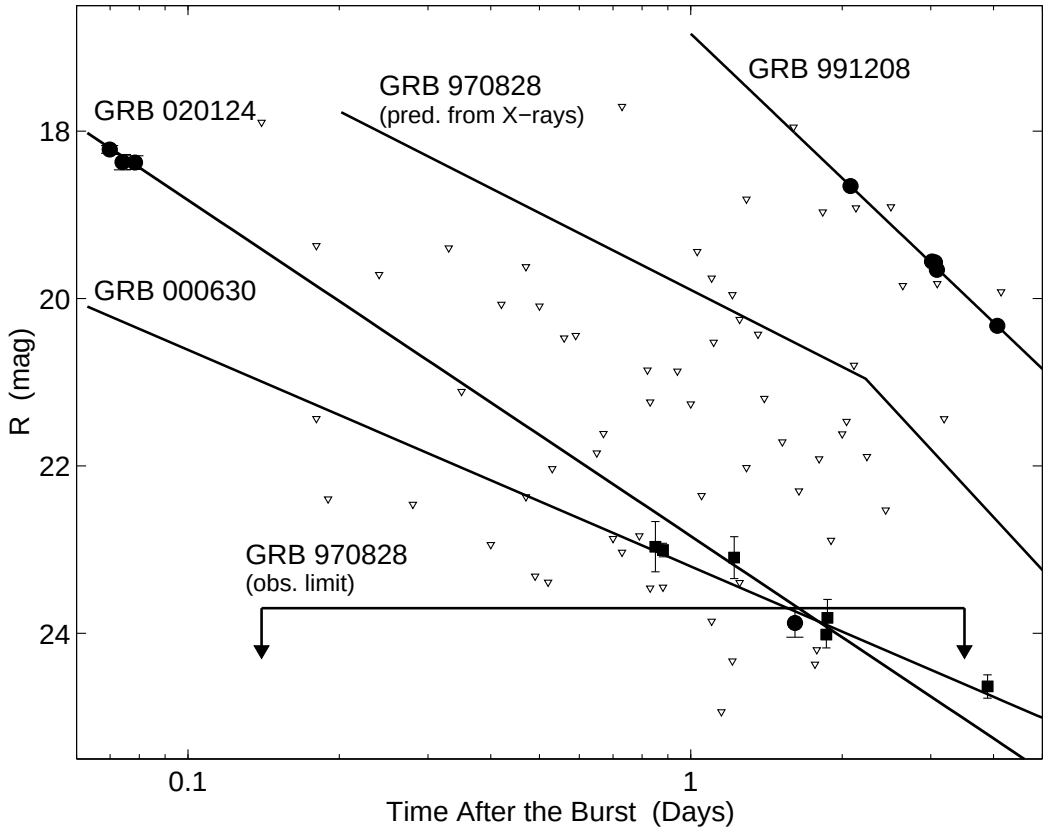

Figure 9.4: R-band upper limits from searches of well-localized GRBs, corrected for Galactic extinction. The limits up to GRB 000630 are taken from Fynbo et al. (2001), while subsequent limits are from the GRB Coordinates Network. Also shown are the light curves of the GRB 020124, GRB 000630, the bright GRB 991208 Castro-Tirado et al. (2001), and GRB 970828 (the de-reddened light curve is based on the radio and X-ray data; Djorgovski et al. 2001a). Only about 30% of the searches yielded limits that are fainter than the afterglow of GRB 020124. A similar fraction was found by Fynbo et al. (2001) based on the afterglow of GRB 000630.

while the J-ISM$_{\rm B}$ and J-Wind$_{\rm B}$ models require values of about 0.05 to 0.3 mag.

We find $t_{\rm jet} \sim 10 - 20$ days, corresponding to $\theta_{\rm jet} \sim 10^{\circ}$. Using the measured fluence (§9.2.1) we estimate the beaming-corrected γ-ray energy, $E_\gamma \approx 5 \times 10^{50}\, n_1^{1/4}$ erg, assuming a circumburst density $n_1 = 1$ cm^{-3} and $z = 1$ (E_γ is a weak function of z). This value is in good agreement with the distribution of E_γ for long-duration GRBs (Frail et al. 2001).

SECTION 9.4

Discussion and Conclusions

Regardless of the specific model for the afterglow emission, the main conclusion of §9.3 is that the optical afterglow of GRB 020124 suffered little or no dust extinction. Still, this afterglow would have been missed by typical searches undertaken even as early as 12 hours after the GRB event. As shown in Figure 9.4, about 70% of the searches conducted to date would have failed to detect an optical afterglow like that of GRB 020124.

This is simply because the afterglow of GRB 020124 was faint and exhibited relatively rapid decay. From Figure 9.5 we note that GRB 020124 is one of the faintest afterglows detected to date (normalized to $t = 1$ day), and while it is not an excessively rapid fader, it is in the top 30% in this category.

Thus, the afterglow of GRB 020124, along with that of GRB 000630 (Fynbo et al. 2001; Figure 9.5)

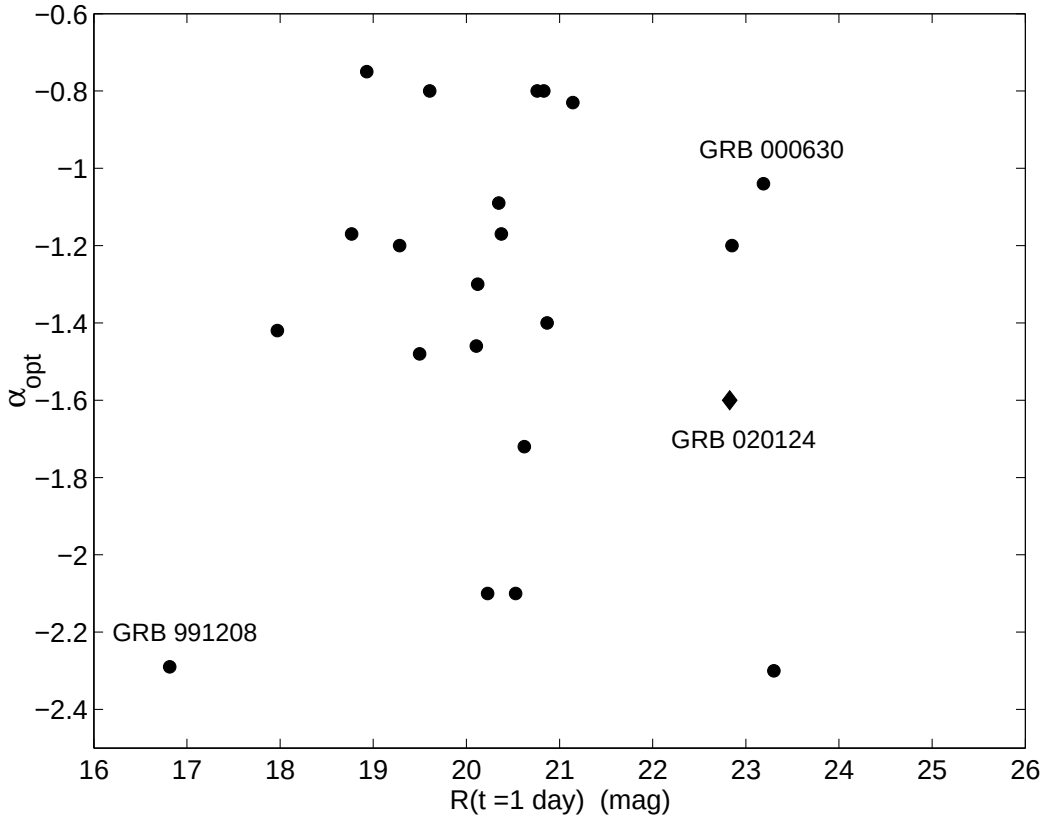

Figure 9.5: Temporal decay index, $\alpha_{\rm opt}$ ($F_\nu \propto t^\alpha$), plotted against the R-band magnitude at $t = 1$ day for several optical afterglows. We chose a fiducial time of 1 day since, with the exception of GRB 010222, all the observations are before the jet break. While the majority of optical afterglows cluster around $R(t = 1\,{\rm d}) \sim 20$ mag, GRB 020124 is one of the four faintest afterglows detected to date, and one of the six most rapid faders.

and GRB 980613 Hjorth et al. (2002), indicates that there is a wide diversity in the brightness and decay rates of optical afterglows. In fact, the brightness distribution spans a factor of about 400, while the decay index varies by more than a factor of three. Coupled with the low dust extinction in the afterglow of GRB 020124, this indicates that some dark bursts may simply be dim, and not dust obscured.

Given this wide diversity in the brightness of optical afterglows, it is important to establish directly that an afterglow is dust obscured. This has only been done in a few cases (§9.1). Therefore, while *statistical* analyses (e.g., Reichart & Yost 2001) point to extinction as the underlying reason for some fraction of dark bursts, it is clear that observationally the issue of dark bursts is not settled, and the observational biases have not been traced fully (see also Fynbo et al. 2001).

Since progress in our understanding of dark bursts will benefit from observations, we need consistent, rapid follow-up of a large number of bursts to constrain the underlying distribution, as well as complementary techniques which can directly measure material along the line of sight. This includes X-ray observations which allow us to measure the column density to the burst (Galama & Wijers 2001), and thus infer the type of environment, and potential extinction level. Along the same line, radio observations allow us to infer the synchrotron self-absorption frequency, which is sensitive to the ambient density (e.g., Sari & Esin 2001); the detection of radio emission, as in the case of GRB 020124, implies a density $n \lesssim 10^2$ cm^{-3}. Finally, prompt optical observations, as we have carried out in this case, may uncover a larger fraction of the dim optical afterglows, and provide a better constraint on the fraction of truly obscured bursts.

J. S. B. is a Fannie and John Hertz Foundation Fellow. F. A. H. acknowledges support from a Presidential Early Career award. S. R. K. and S. G. D. thank the NSF for support. R. S. is grateful for support from a NASA ATP grant. R. S. and T. J. G. acknowledge support from the Sherman Fairchild Foundation. J. C. W. acknowledges support from NASA grant NAG59302. K. H. is grateful for Ulysses support under JPL contract 958056 and for IPN support under NASA grants FDNAG 5-11451 and NAG 5-17100. Support for Proposal HST-GO-09180.01-A was provided by NASA through a grant from the Space Telescope Science Institute, which is operated by the Association of Universities for Research in Astronomy, Inc., under NASA contract NAS5-26555. We thank the anonymous referee for helpful comments.

Table 9.1. Ground-Based Optical Observations of GRB 020124

UT	Telescope	Band	Magnitude
Jan 24.51204	MSO 50	R_M	17.918 ± 0.041
Jan 24.51204	MSO 50	B_M	18.628 ± 0.057
Jan 24.51516	SSO 40	R	18.219 ± 0.046
Jan 24.51655	MSO 50	R_M	17.984 ± 0.044
Jan 24.51655	MSO 50	B_M	18.727 ± 0.063
Jan 24.51938	SSO 40	R	18.371 ± 0.091
Jan 24.52106	MSO 50	R_M	18.111 ± 0.049
Jan 24.52106	MSO 50	B_M	18.842 ± 0.069
Jan 24.52373	SSO 40	R	18.376 ± 0.082
Jan 24.55791	MSO 50	R_M	18.678 ± 0.048
Jan 24.55791	MSO 50	B_M	19.661 ± 0.090
Jan 24.56243	MSO 50	R_M	18.867 ± 0.036
Jan 24.56243	MSO 50	B_M	19.584 ± 0.053
Jan 24.56696	MSO 50	R_M	18.843 ± 0.039
Jan 24.56696	MSO 50	B_M	19.714 ± 0.050
Jan 26.34100	P 200	r'	24.398 ± 0.228

Note. — The columns are (left to right), (1) UT date of each observation, (2) telescope (MSO 50: Mt. Stromlo Observatory 50-in; SSO 40: Siding Spring Observatory 40-in; P 200: Palomar Observatory 200-in), (3) observing band, and (4) magnitudes and uncertainties. The observed magnitudes are not corrected for Galactic extinction.

Table 9.2. HST/STIS Observations of GRB 020124

Epoch (UT)	Band	Exp. Time (ksec)	Flux (e^- s^{-1})	S/N	Magnitude
Feb 11.09	50 CCD/Clear	10.0	0.0814 ± 0.0169	4.82	$R = 28.68^{+0.25}_{-0.20}$
Feb 18.30	50 CCD/Clear	7.4	0.0443 ± 0.0189	2.34	$R = 29.35^{+0.60}_{-0.39}$
Feb 25.71	50 CCD/Clear	7.5	0.0362 ± 0.0183	1.98	$R = 29.56^{+0.76}_{-0.44}$
Feb 18.30+25.71	50 CCD/Clear	14.9	0.0398 ± 0.0137	2.91	$R = 29.46^{+0.46}_{-0.32}$

Note. — The columns are (left to right), (1) UT date of each observation, (2) STIS CCD mode, (3) exposure time, (4) flux and uncertainty, (5) significance, and (6) R magnitude and uncertainty. The total number of counts was converted to the R-band assuming the observed color of the OT, $f_\lambda \propto \lambda^{-0.5}$ (§9.2.2). The R-band errors reflect only the statistical uncertainty. Choosing a wide range of assumed colors for the afterglow ($\alpha_\lambda = -2.5$ to 0.5) gives $+0.25$, -0.05 mag. Thus, the afterglow could not have been much brighter in R-band than reported in epoch 1. We include this color uncertainty in the analysis (§9.3), and in Figure 9.3, choosing half of the range as the rms of the systematic color uncertainty. In addition, we also include in the analysis the estimated uncertainty from the aperture correction (0.1 mag; §9.2.2). For epochs 2 and 3, the 3σ upper limits are: $R = 29.09$ and $R = 29.13$ mag, respectively. The observed magnitudes are not corrected for Galactic extinction.

Table 9.3. VLA Radio Observations of GRB 020124

Epoch (UT)	ν_0 (GHz)	Flux Density (μJy)
Jan 26.22	8.46	84 ± 30
Jan 26.25	22.5	-60 ± 100
Jan 27.22	8.46	45 ± 25
Feb 1.40	8.46	49 ± 17
Jan 26.22-Feb 1.40	8.46	48 ± 13

Note. — The columns are (left to right), (1) UT date of each observation, (2) observing frequency, and (3) flux density at the position of the radio transient with the rms noise calculated from each image. The last row gives the flux density at 8.46 GHz from the co-added map.

Table 9.4. Afterglow Models for GRB 020124

Model	α_1	α_2	β	(b, c)	Closure	p	$A_V^{\rm host}$ (mag)
$\rm ISM_B$	$-\frac{3(p-1)}{4}$	$-\frac{3p}{4}+\frac{1}{2}$	$-\frac{p-1}{2}$	$(-3/2, 0)$	0.52 ± 0.28	3.17 ± 0.05	(0.35, 0.18, 0.10)
$\rm Jet_B$	$-p$	$-p$	$-\frac{p-1}{2}$	$(-2, 1)$	2.23 ± 0.36	1.63 ± 0.04	(0.89, 0.50, 0.22)
$\rm J\text{-}ISM_B$	$-\frac{3(p-1)}{4}$	$-p$	$-\frac{p-1}{2}$	$(-3/2, 0)$	0.52 ± 0.28	3.17 ± 0.05	(0.30, 0.10, 0.05)
$\rm J\text{-}Wind_B$	$-\frac{3p-1}{4}$	$-p$	$-\frac{p-1}{2}$	$(-3/2, 1/2)$	1.02 ± 0.28	2.51 ± 0.05	(0.30, 0.16, 0.08)
$\rm J\text{-}ISM/Wind_R$	$-\frac{3p-2}{4}$	$-p$	$-\frac{p}{2}$	$(-3/2, -1/2)$	0.02 ± 0.28	2.84 ± 0.05	—

Note. — The columns are (left to right), (1) Afterglow model (ISM: r^0 circumburst medium; Wind: r^{-2} circumburst medium; Jet: collimated eject with opening angle $\theta_{\rm jet}$; a subscript B indicates $\nu_c < \nu_{\rm opt}$, and a subscript R indicates $\nu_c > \nu_{\rm opt}$), (2) α_1 as a function of p, (3) α_2 as a function of p, (4) β as a function of p, (5) closure relations ($\alpha + b\beta + c = 0$), (6) resulting closure values from the observed values of α_1 and β, (7) inferred value of p from the measured value of α_1, and (8) the required extinction in the frame of the host galaxy for closure values of zero ($z = 0.3$, 1, 3); typical uncertainties are ± 0.05 mag. The top two models apply to the case when the observed steepening in the light curves is due to the passage of ν_c through the R-band, while the bottom three apply to the case when the steepening is due to a jet.

Table 9.5. Limits on Optical Afterglow Magnitudes for Bursts Localized in 2000–2002

GRB	Epoch (days)	R-limit (mag)	Reference
GRB 000801	1.77	24.5	GCN 767
GRB 000812	4.14	20.8	GCN 771
GRB 000830	0.99	24.5	GCN 788
GRB 001025	1.21	24.5	GCN 867
GRB 001204	3.09	20.1	GCN 898
GRB 010103	1.83	19.2	GCN 911
GRB 010119	1.13	18	GCN 919
GRB 010126	0.88	23.5	GCN 926
GRB 010214	0.83	21.3	GCN 949
GRB 010220	0.35	23.5	GCN 958
GRB 010324	1.29	22.3[a]	GCN 1024
GRB 010326A	0.50	21.5	GCN 1022
GRB 010412	0.60	20.5[a]	GCN 1039
GRB 011019	1.15	25.0	GCN 1128
GRB 011212	2.0	24.0	GCN 1324
GRB 020127	0.18	19.5	GCN 1230
GRB 020409	1.25	23.5	GCN 1362

Note. — The columns are (left to right), (1) GRB name, (2) observing time after the burst, (3) R-band limit, and (4) GCN circular reference.

[a] V-band limit

CHAPTER 10

The Host Galaxy of GRB 980703 at Radio Wavelengths — A Nuclear Starburst in a ULIRG†

E. Berger[a], S. R. Kulkarni[a], & D. A. Frail[b]

[a]Department of Astronomy, 105-24 California Institute of Technology, Pasadena, CA 91125, USA

[b]National Radio Astronomy Observatory, P. O. Box 0, Socorro, NM 87801

Abstract

We present radio observations of GRB 980703 at 1.43, 4.86, and 8.46 GHz for the period of 350 to 1000 days after the burst. These radio data clearly indicate that there is a persistent source at the position of GRB 980703 with a flux density of approximately 70 μJy at 1.43 GHz, and a spectral index, $\beta \approx 0.32$, where $F_\nu \propto \nu^{-\beta}$. We show that emission from the afterglow of GRB 980703 is expected to be one to two orders of magnitude fainter, and therefore cannot account for these observations. We interpret this persistent emission as coming from the host galaxy — the first example of a γ-ray burst (GRB) host detection at radio wavelengths. We find that it can be explained as a result of a star formation rate (SFR) of massive stars ($M > 5$ M$_\odot$) of ≈ 90 M$_\odot$/yr, which gives a total SFR (0.1M$_\odot$ <M< 100M$_\odot$) of ≈ 500 M$_\odot$/yr. On the basis of these data alone we cannot rule out that some fraction of the radio emission originates from an obscurred active galactic nucleus. Using the correlation between the radio and far-IR (FIR) luminosities of star-forming galaxies, we find that the host of GRB 980703 is at the faint end of the class of Ultra Luminous Infrared Galaxies (ULIRGs), with $L_{FIR} \sim 10^{12}$ L$_\odot$. From the radio measurements of the offset between the burst and the host, and the size of the host, we conclude that GRB 980703 occurred near the center of the galaxy in a region of star formation. A comparison of the properties of this galaxy with radio and optical surveys at a similar redshift ($z \approx 1$) reveals that the host of GRB 980703 is an average radio-selected star-forming galaxy. This result has significant implications for the potential use of a GRB-selected galaxy sample for the study of galaxies and the IGM at high redshifts, especially using radio observations, which are insensitive to extinction by dust and provide an unbiased estimate of the SFR through the well-known radio-FIR correlation.

SECTION 10.1

Introduction

Recent studies of the properties and host galaxies of γ-ray bursts (GRBs) reveal some indirect evidence for the link between GRBs and star formation. Optical measurements of the offset distribution of GRBs

† A version of this chapter was published in *The Astrophysical Journal*, vol. 560, 652–658, (2001).

from their host centers appears to be consistent with the distribution of collapsars in an exponential disk, but inconsistent with the expected offset distribution of delayed binary mergers (Bloom et al. 2002a). GRB 990705 is an illustrative example of this result since HST images revealed that the burst was situated in a spiral arm, just north of an apparent star forming region (Holland et al. 2001; Bloom et al. 2002a). The absence of optical afterglows from the so-called "dark GRBs" (Djorgovski et al. 2001a) points to the association of GRBs with heavily obscured, and possibly star-forming, regions. In addition, Galama & Wijers (2001) claim high column densities toward several GRBs from X-ray observations of afterglows

Consequently, one of the pressing questions in the study of GRB host galaxies is whether they are representative of star-forming galaxies at a similar redshift. If they are, then the dust-penetrating power of GRBs and their broad-band afterglow emission offer a number of unique diagnostics of their host galaxies: the obscured star formation fraction, the ISM within the disk, the local environment of the burst itself, and global and line-of-sight extinction, to name a few.

GRB 980703, which has one of the brightest (apparent magnitude) hosts to date ($R \approx 22.6$ mag; Bloom et al. 1998a; Vreeswijk et al. 1999) offers an excellent opportunity for detailed studies. The afterglow optical and near-IR (NIR) light curves exhibited pronounced flattening about 6 days after the burst and this was attributed to an underlying bright host (Bloom et al. 1998a; Castro-Tirado et al. 1999; Vreeswijk et al. 1999). Djorgovski et al. (1998) undertook spectroscopic observations of the host and obtained a redshift of 0.966. Using three different estimators ([OII], Hα and 2800Å UV continuum) of the star formation rate (SFR), Djorgovski et al. (1998) inferred extinction-corrected SFR of 10 to 30 $M_\odot$/yr.

Here we report radio observations of GRB 980703 covering the period 350–1000 days after the burst at three frequencies: 1.43, 4.86, and 8.46 GHz. This burst has the distinction of being followed up for 1000 days; the previous record-holder was GRB 970508 (445 days; Frail et al. 2000c). The organization of the paper is as follows. We summarize the radio observations and data reduction in §10.2. In §10.3 we summarize the main observational results. In §10.4 we show that the late time radio observations require a steady component over and above the decaying afterglow observations. We argue that this component is unlikely to arise from an unobscured AGN but is instead due to star formation. In §10.5, we infer the SFR from the radio observations and compare and contrast this estimate to those derived from optical observations. Thanks to the high angular resolution and accurate astrometry of radio observations we are able to derive an accurate offset between the burst and the centroid of the host, as well as constrain the size of the radio emitting region (§10.6).

SECTION 10.2

Radio Observations

Very Large Array (VLA[1]) observations of GRB 980703 were initiated on 1998, July 4.40 UT at 4.86 GHz. All observations were obtained in the standard continuum mode with 2×50 MHz contiguous bands. We used the extra-galactic sources J2330+110, J0010+109 and J0022+061 for phase calibration and 3C48 (J0137+331) and 3C147 (J0542+498) for flux calibration. We used the Astronomical Image Processing System (AIPS) for data reduction.

Late-time observations (time after the burst, $t \gtrsim 350$ days) were co-added over a period of a few to thirty days in order to increase the overall sensitivity of each detection. This is appropriate since the expected change in the flux density from the afterglow over a few days, several hundred days after the burst, is negligible relative to the associated errors in the measurements. A log of the late-time observations and the flux density measurements are summarized in Table 10.1, and the light curves are shown in Figure 10.1. A summary of the early radio data, as well as broad-band modeling is given in Frail et al. (2003b).

[1] The VLA is operated by the National Radio Astronomy Observatory (NRAO), a facility of the National Science Foundation operated under cooperative agreement by Associated Universities, Inc.

SECTION 10.3

Results

From Figure 10.1, we see that the late-time ($t \gtrsim 350$ days) radio light curves do not exhibit the customary power-law decay expected of afterglows but instead show flattening. Using all the measurements in Table 10.1, we find the following weighted-average flux densities for the host galaxy of GRB 980703: $F_{\nu,8.46} = 39.3 \pm 4.9$ μJy, $F_{\nu,4.86} = 42.1 \pm 8.6$ μJy, and $F_{\nu,1.43} = 68.0 \pm 6.6$ μJy. We searched for, but did not find, evidence for significant variability over the 650 day monitoring period (see Figure 10.2). From these flux densities we find that the radio spectral index is $\beta = 0.32 \pm 0.12$, where $F_\nu \propto \nu^{-\beta}$.

These radio images also allow us to determine the projected angular offset between the host galaxy and afterglow of GRB 980703. For each individual detection positions were determined from Gaussian fits, and the host-GRB offset was calculated with respect to a Very Long Baseline Array (VLBA) position that was measured to 0.0007 arcsec accuracy in each coordinate on 1998 August 2 at 8.42 GHz. These offsets are displayed in Figure 10.3 and the combined value from all observing runs is shown in the insert. We find an average offset from all measurements of -0.032 ± 0.015 arcsec in RA and 0.024 ± 0.015 arcsec in declination. The uncertainty in the position of the source is given by $\delta\theta_{\rm offset} \approx (\theta_{synbeam}/2)/(S/N)$, where $\theta_{synbeam} \approx \lambda/B_{max}$ is the half-power synthesized beam-width, λ is the observing wavelength, B_{max} is the length of the maximum baseline, and S/N is the signal-to-noise ratio of the flux measurement.

The optical measurements of Bloom et al. (2002a) for the host of GRB 980703, give an angular offset of -0.054 ± 0.055 in RA and 0.098 ± 0.065 in declination (see insert in Figure 10.3). They conclude that GRB 980703 was not significantly offset from the center of its host galaxy, in agreement with the more accurate offset measurements in the radio.

In addition to accurate measurements of the offset, the radio observations allow us to place meaningful limits on the size of the radio-emitting region (i.e., the size of the star-forming region). We find that in our highest resolution images the source is unresolved, and therefore, based on the synthesized beam size we can derive an upper limit on the physical size of the source. For our adopted cosmological parameters (section 10.5) we find that the angular diameter distance to the source is $d_A \approx 5.4 \times 10^{27}$ cm. The full synthesized beam-width at 8.46 GHz is $\theta_{HPBW} \approx 0.27$ arcsec, which gives an upper limit of $D_{rad} = d_A \theta_{HPBW} < 2.3$ kpc on the diameter of the source.

SECTION 10.4

Evidence for Host Galaxy Emission in the Radio Regime

An afterglow origin is difficult to reconcile with the properties of the late-time radio emission. From the early broad-band data it was inferred that the afterglow spectrum peaked at frequency, $\nu_m \sim 4 \times 10^{12}$ Hz at $t = 1.2$ days (Vreeswijk et al. 1999). If the explosion was spherical then we expect $\nu_m \propto t^{-3/2}$ (Sari et al. 1998; Chevalier & Li 2000). Thus the radio emission at 8.46 GHz is expected to decay for $t > 70$ days after the burst, while the emission at 1.43 GHz will decay for $t > 240$ days after the burst. If the ejecta were collimated (opening angle, θ_j), then we expect a more rapid decay, $\nu_m \propto t^{-2}$, once the bulk Lorentz factor, Γ, of the flow falls below θ_j, $\Gamma(t) \lesssim \theta_j^{-1}$ (Sari et al. 1999). In this case, we expect the radio afterglow to start decaying at even earlier times, and the flux will decay faster relative to a spherical explosion. In either case, we expect the radio afterglow to decay by at least a factor of three over the time span under consideration, $350 < t < 1000$ days.

We can clearly see from Figure 10.1 that this decay is not taking place, and the flux instead remains constant over a period of approximately 650 days. This behavior is similar to the flattening observed in the optical/NIR light curves of several GRBs (including GRB 980703), when the emission from the afterglow decays below the level of emission from the host galaxy.

Furthermore, the afterglow spectrum is expected to be a power law, $F_\nu \propto \nu^{-\beta}$, where $\beta = (p-1)/2$ and p is the power law index of the Lorentz factor distribution of the shocked electrons, $N(\gamma)d\gamma \propto \gamma^{-p}d\gamma$

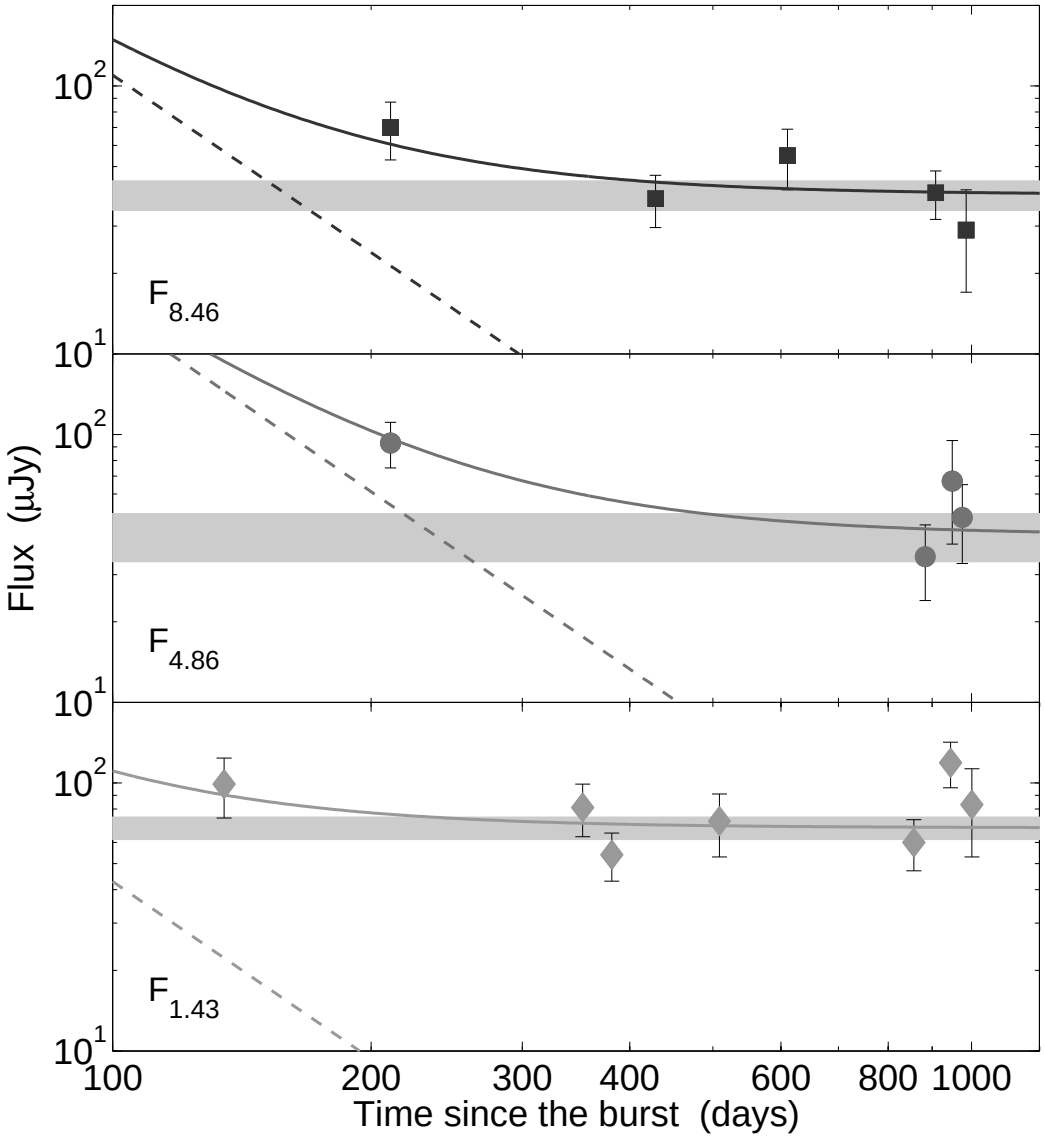

Figure 10.1: Radio light curves at 1.43, 4.86, and 8.46 GHz. The thin solid lines are the combined afterglow and host galaxy emission, the dotted lines indicate the afterglow emission, and the thick solid lines are the weighted-average fluxes of the host galaxy, with the thickness indicating the uncertainty in the flux. Only measurements at $t \gtrsim 350$ days after the burst were used to calculate the host flux. The fits are based on broad-band fitting. The data clearly indicate that there is a constant component in the observed emission, interpreted as the host galaxy.

for $\gamma > \gamma_{\rm min}$ (Sari et al. 1998). From the observations of many afterglows, we note that p is in the range 2.2 to 2.6 and thus we expect $\beta \sim 0.7$; for GRB 980703 the spectral index inferred from the optical data by several groups ranges from $0.6 - 1$ (Bloom et al. 1998a; Castro-Tirado et al. 1999; Vreeswijk et al. 1999). However, the observed spectral index in the range 1.43–8.46 GHz is much lower, $\beta = 0.32 \pm 0.12$. We thus conclude that there exists a steady source of emission other than the afterglow.

It is instructive to compare the characteristics of the radio emission toward GRB 980703 with those of other galaxies at a similar redshift. A radio survey of the Hubble Deep Field (HDF) and its flanking fields showed that the mean spectral index of the 8.46 GHz selected sample is $\langle \beta_{8.46} \rangle = 0.35 \pm 0.07$ (Richards 2000). In a survey of two $7' \times 7'$ fields with the VLA at 8.44 GHz Windhorst et al. (1993) found for sources with a flux density $\lesssim 100$ μJy (hereafter, μJy sources) a median spectral index,

$\beta_{\rm med} \approx 0.35 \pm 0.15$, and Fomalont et al. (1991) found $\beta_{\rm med} \approx 0.38$ for μJy sources selected at 4.9 GHz. Thus, the host galaxy of GRB 980703 appears to be a normal μJy source compared to sources selected at 4.9 or 8.5 GHz. In addition, it has been noted (Richards 2000) that the spectral index of radio sources selected at frequencies larger than 5 GHz flattens from a value of approximately 0.7 for the mJy ($F_\nu \gtrsim 1$ mJy) population to 0.3 for μJy sources.

The reason for the flattening of the spectral index may be due to the varying ratio of thermal bremsstrahlung to synchrotron emission for galaxies undergoing a burst of star formation. Supernova remnant shock acceleration of electrons results in synchrotron emission, with a characteristic spectral index of ≈ 0.8 (Condon 1992). On the other hand, thermal bremsstrahlung emission from HII regions, excited by star formation, has a much flatter spectral index, $\beta \approx 0.1$. Thus, as the direct contribution from massive stars increases the spectra are expected to flatten from a value of 0.8 to 0.1. This is exactly the effect that is observed in the aforementioned surveys.

Within the HDF and SSA13 Richards et al. (1999) identified radio sources with fluxes in the range 10–100 μJy with bright disk galaxies with $I \approx 22$ mag. The $I-K$ color for these galaxies is approximately 2.5 mag. Bloom et al. (1998a) find $I \approx 21.9$ mag and $I-K \approx 2.1$ mag for the host of GRB 980703. Thus, we see from both the radio spectrum of the source, and the optical I mag and $I-K$ color that the host galaxy of GRB 980703 has the characteristics of a typical star-forming radio galaxy selected at 8.5 GHz.

An alternate explanation for the radio emission is that it originates from an active galactic nucleus (AGN). It has been noted in surveys of the Hubble Deep Field (HDF), its flanking fields, and the Small Selected Area 13 (SSA13) that approximately 20% of the radio sources are AGN with spectral indices of about 0.3 (Richards et al. 1999; Richards 2000; Barger et al. 2000). Windhorst et al. (1993) found a similar result in their survey of two $7' \times 7'$ fields at 8.44 GHz. Thus, there is a modest probability that the emission from the host of GRB 980703 is due to an AGN.

We consider the AGN hypothesis unlikely based on the radio data and optical spectroscopy. Optical spectra of the source obtained by Djorgovski et al. (1998) show no evidence for an unobscured AGN: high-ionization lines such as Mg II λ2799, [NeV]λ3346, and [NeV]λ3426 are absent, and the [OIII]λ4959 to Hβ ratio is approximately 0.4, much lower than [OIII]/H$\beta > 1.3$ for AGN (Rola et al. 1997). Another way to discriminate between AGN and star-forming galaxies is to correlate the [OII] equivalent width (EW) with continuum color (Dressler & Gunn 1982). Kennicutt (1992) showed that AGN have redder colors for similar [OII] EW, relative to normal galaxies. Using the spectrum presented in Djorgovski et al. (1998) we evaluate the color index, $(41-50) \equiv 2.5\log[f_\nu(5000\text{Å})/f_\nu(4100\text{Å})]$ (Kennicutt 1992), and find it to be 0 ± 0.1; an AGN with the same [OII] EW would have a value $\gtrsim 0.3$ (Kennicutt 1992). Finally, Rola et al. (1997) found that for a sample of emission-line galaxies at $z \sim 0.8$, the color index between the continuum underlying the Hβ and [OII]λ3727 lines is ≥ 0.4 for all AGN in their sample. Using the spectrum of Djorgovski et al. (1998) we find that this color index is approxmiately zero.

A second, though less persuasive argument against an AGN origin is the apparent absence of significant radio variability over the 650 day monitoring period (see Figure 10.2). The radio cores of most, but not all, low-luminosity AGN show variability exceeding the observed levels (Falcke et al. 2001).

In summary, we conclude that the radio emission seen from the host of GRB 980703 is dominated by star formation. We note, however, that the arguments presented above are not sufficient to rule out the presence of an *obscured* AGN. Determining the degree to which active star formation and/or a central engine contribute to the total emission is a common problem with centimeter and submillimeter-selected galaxies (e.g., Ivison et al. 2000). X-ray observations by *Chandra* or *XMM* may be needed to conclusively show which is the dominant power source. In the next section we assume that the bulk of the radio emisison is due to star formation and show that the host is a typical radio galaxy at $z \sim 1$ undergoing star formation.

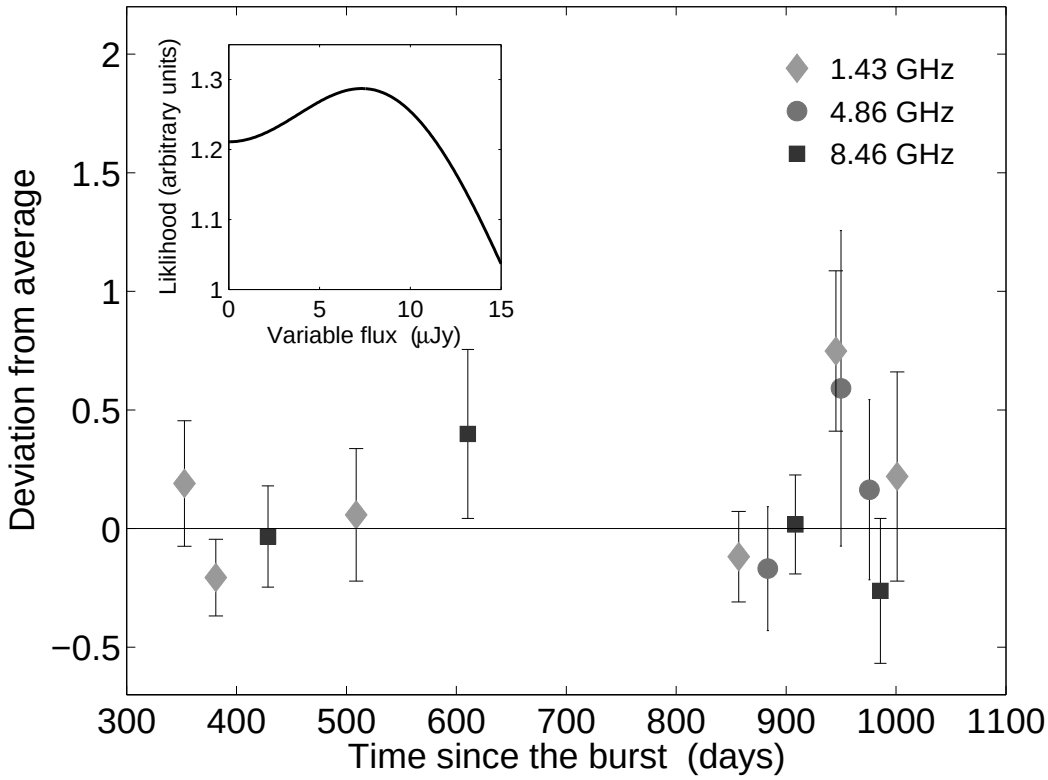

Figure 10.2: Fluctuations of individual measurements around the weighted average presented by the wide strips in figure 10.1. We note that there are no fluctuations above 1.1σ at 8.46 GHz, 0.8σ at 4.86 GHz, and 1.7σ at 1.43 GHz, indicating that the flux in each band is consistent with a constant. In fact, if we assume that the source has some variability (over that due to measurement errors), then the variable flux is less than ± 7 μJy, with a 40% probability that there are no fluctuations at all (see insert). This conclusion supports the hypothesis that the radio emission is not due to an unobscured AGN.

SECTION 10.5

The Star Formation Rate in the Host Galaxy of GRB 980703

Star formation is traced by optical, far-IR, submillimeter, and radio emission. In the following we will use the radio data to estimate the SFR in the host galaxy of GRB 980703, and then compare the results with the SFR derived from optical indicators, and with radio surveys at a similar redshift range in order to place the host of GRB 980703 in a larger context.

10.5.1 Star Formation Rate from the Radio Observations

Condon (1992) showed that the total radio luminosity is a combination of synchrotron and thermal emission components, both directly related to the formation rate of massive stars via a simple relationship. Moreover, since the lifetime of massive stars is of the order of 10^7 years, and the lifetime of the synchrotron emitting electrons is of the order of 10^8 years (Condon 1992), the radio emission is an excellent probe of the instantaneous SFR.

From the redshift of GRB 980703, $z = 0.966$ (Djorgovski et al. 1998), and the cosmological parameters $\Omega_0 = 0.3$, $\Lambda_0 = 0.7$ and $H_0 = 65$ km/sec/Mpc, we find that the luminosity distance to the burst is $d_L = d_A(1+z)^2 \approx 2.1 \times 10^{28}$ cm, and the observed luminosity at each frequency is given by $L_\nu = 4\pi d_L^2 F_\nu$. The emitted luminosity is given by $L_{em,\nu'} = L_{obs,\nu}(\nu/\nu')^\beta (1+z)^\beta$, where β is the spectral index of the radio emission, ν' is the source-frame frequency, and ν is the observing frequency. The radio spectral index derived in §10.3 is $\beta = 0.32 \pm 0.12$, and thus the emitted luminosity in each

frequency is approximately 25% higher than the observed luminosity at the same frequency.

The emitted luminosity at $\nu' = 1.43$ GHz is $L_{em}(1.43) = (4.7 \pm 0.6) \times 10^{30}$ erg sec^{-1}, and we find that the SFR of massive stars in the host of GRB 980703 is

$$\mathrm{SFR}(\mathrm{M}>5\mathrm{M}_\odot) \approx \frac{L_{em}(1.43)}{5.3 \times 10^{28} \nu'^{-\beta}_{\mathrm{GHz}} + 5.5 \times 10^{27} \nu'^{-0.1}_{\mathrm{GHz}}} \approx 90 \mathrm{M}_\odot/\mathrm{yr}. \quad (10.1)$$

Since both the thermal and non-thermal components are proportional only to the formation rate of high-mass stars, Equation 10.1 has to be modified by a factor which accounts for the contribution from stars in the mass range 0.1–5 $M_\odot$. For a Salpeter IMF this factor evaluates to 5.5. We use the Salpeter IMF since it is already implicitly used in equation 10.1 for the mass range 5–100 $M_\odot$. Thus, within this framework the total SFR is ≈ 500 $M_\odot$/yr.

Haarsma et al. (2000) derived the SFR for radio galaxies in the HDF, its flanking fields, SSA13, and V15 in the redshift range $0.85 - 1.15$. These fields have been observed to μJy sensitivities at cm wavelengths, and the detected radio sources have been identified with optical sources for which the redshift was determined. We use their flux and spectral index measurements along with Equation 10.1 and the correction factor to calculate the total SFR for each galaxy, and we derive a mean SFR $= 657 \pm 106$ $M_\odot$/yr. It is clear that the host of GRB 980703 is an average star-forming radio galaxy at $z \approx 1$. This conclusion meshes well with the comparison of the radio spectral index, optical I mag, and optical $I - K$ color of the host of GRB 980703 to the same sample (see §10.4).

10.5.2 Star Formation Rate from Optical and Submillimeter Data

Djorgovski et al. (1998) used Hα and the 2800Å UV continuum to calculate a SFR of approximately 10 $M_\odot$/yr in the host of GRB 980703, after correcting for rest-frame extinction, $A_V \approx 0.3$ mag. Sokolov et al. (2001) found a similar intrinsic extinction, $A_V \approx 0.3 - 0.65$, and based on template spectral energy distributions found that the best model for the broad-band optical spectrum is given by exponentially decreasing star formation with an extinction-corrected SFR of 20 $M_\odot$/yr.

Clearly, the SFR derived from optical indicators is much lower than the value from radio measurements, even after correcting for extinction. This result is part of a general trend that has been observed in galaxies with SFR $\gtrsim 0.1$ $M_\odot$/yr (Hopkins et al. 2001). Hopkins et al. (2001) propose dust reddening dependent on SFR as the solution to this problem, and we therefore expect a much better result if we use their prescription. Extending their correlation to $\mathrm{SFR}_{1.43} \approx 500$ $M_\odot$/yr, we find that the predicted observed SFR from Hα is approximately 70 $M_\odot$/yr. This value is still much higher than the measured SFR. In fact, in the Hopkins et al. (2001) sample the optically-derived SFR rarely exceeds 10 $M_\odot$/yr, while the radio-derived values go up to several hundred $M_\odot$/yr, indicating that the optical emission does not trace the entire star-forming volume. Thus, the SFR values for this particular galaxy are not unexpected.

The submillimeter (e.g., 350 GHz) emission from galaxies serves as another estimator of SFR, and it is related to the radio emission at 1.43 GHz via a redshift-dependent spectral index, $\beta^{350}_{1.4}$ (Carilli & Yun 1999, 2000; Dunne et al. 2000). Using the value from Carilli & Yun (2000), $\beta^{350}_{1.4} \approx 0.54 \pm 0.16$ at $z \approx 0.97$, we find $F_\nu(350) \approx 1.3^{+1.9}_{-0.8}$ mJy. Observations with the Submillimeter Common User Bolometer Array (SCUBA) camera on the James Clark Maxwell Telescope (JCMT) 12.4 days after the burst provided a 2σ upper limit of 3.2 mJy on the combined emission from the afterglow and host at 350 GHz (Smith et al. 1999), consistent with the predictions from the radio-submillimeter relation.

To conclude, we use the derived SFR to calculate the expected far-IR (FIR) emission from the host of GRB 980703. The luminosity of the FIR radiation can be derived from the empirical relation suggested by Helou et al. (1985),

$$q = -12.6 + \log(F_{FIR}/F_{1.4}) \approx 2.3 \quad (10.2)$$

which evaluates to $L_{FIR} \approx 1.5 \times 10^{12}$ $L_\odot$ for the host of GRB 980703; here F_{FIR} is the total flux in the range 40–120 μm in units of erg sec^{-1} cm^{-2}, and $F_{1.4}$ is the flux density at 1.4 GHz in units of erg sec^{-1} cm^{-2} Hz^{-1}. This value of the FIR luminosity places the host galaxy of GRB 980703 in the category of ULIRG (Sanders & Mirabel 1996). A similar claim was made for the host galaxy of GRB 970508 (Hanlon et al. 2000); however, the 41" diameter beam of the Infrared Space Observatory prevents a conclusive association of the detected 60 μm source with the host galaxy.

SECTION 10.6

Offsets and Source size

Holland et al. (2001) used a $R^{1/n}$ profile to fit the optical emission from the host and found that the best fit gives a half-light radius of 0.13 arcsec, which corresponds to an exponential disk with a scale-diameter of 0.44 arcsec. Thus, the physical size of the galaxy is $D_{opt} \approx 3.7$ kpc, 60% larger than the upper limit from our radio measurements. Holland et al. (2001) claim that the center of the galaxy is 0.2 mag bluer than the outer regions of the host. If so, star formation must be mainly taking place within the inner parts of the galaxy. Since the radio emission directly traces current star formation, we expect the radio emission to be more centrally concentrated than the optical emission. Thus, as expected, the radio size of the galaxy is smaller than the optical size.

Most likely the GRB is located within the nuclear starburst given the small offset of the GRB from the centroid of the galaxy. If so it raises the question of why the afterglow was not completely extinguished by dust. In fact, in order to reconcile the optical and radio derived SFRs we require a rest-frame extinction of $A_V \sim 4.5$ mag. Observations of the afterglow, which provide an estimate of extinction along the line-of-sight to the burst, give values of 1–2 mags from optical observations, and a somewhat higher (but highly uncertain) value from X-ray observations (Bloom et al. 1998a; Castro-Tirado et al. 1999; Vreeswijk et al. 1999). Thus, the extinction in the nuclear star-forming region is higher than the average over the whole galaxy, and the correction to the observed optical SFR is almost sufficient to reconcile it with the value of 500 $M_\odot$/yr derived from the radio.

The relatively small source size also agrees well with the classification of the host of GRB 980703 as a ULIRG exhibiting a starburst. Kennicutt (1998) showed that star formation with a rate $\gtrsim 20$ $M_\odot$/yr invariably takes place in circumnuclear regions of size 0.2–2 kpc, in the form of nuclear starburst. As a result, we expect that ULIRGs will have such size scales when traced by star formation, and the source size we measured for the host of GRB 980703 indicates that it is probably undergoing a nuclear starburst.

Finally, from the source size and offset measurement we conclude that GRB 980703 took place inside the star-forming region, providing further indirect evidence linking GRBs to massive stars

SECTION 10.7

Discussion and Conclusions

Late-time observations of GRB 980703 reveal a steady component, with a flux density $F_{\nu,1.43} = 68.0 \pm 6.6$ μJy and a spectral index $\beta = 0.32 \pm 0.12$. The spectral and temporal characteristics of this emission indicate that it does not arise from the afterglow itself, but rather it is the result of star formation in the host galaxy, with SFR ≈ 500 $M_\odot$/yr. This leads to the interpretation that this host galaxy is a ULIRG undergoing a starburst. In addition, the star formation is concentrated within the inner two kpc of the host, and the progenitor of GRB 980703 was positioned within this region of star formation. This conclusion lends additional support for the collapsar model.

If GRBs really come from massive stars, then they can be used to trace the star formation history of the universe (e.g., Wijers et al. 1998). In addition, GRBs and their afterglows are potentially detectable out to very high redshifts (Lamb & Reichart 2000). These propositions, taken together with the dust-penetrating power of their γ-ray emission, make GRBs a unique tool for the study of galaxies and the

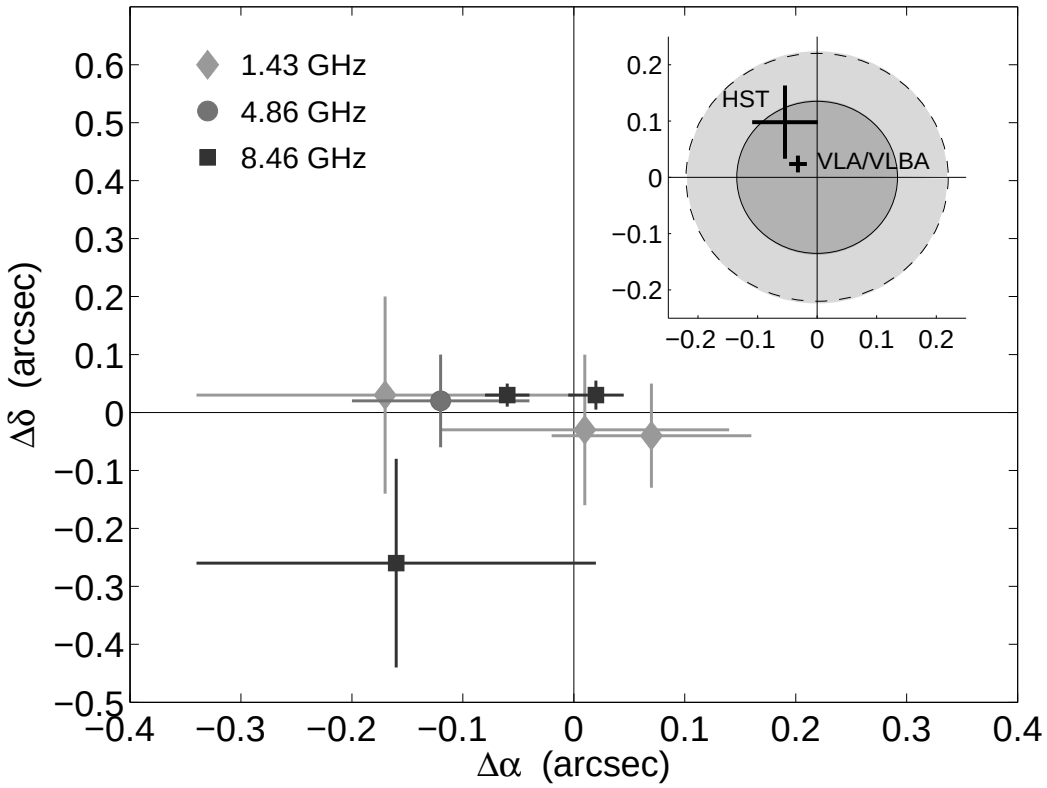

Figure 10.3: Offset measurements for all epochs in which the host galaxy emission dominates, and for which the measurements are accurate to more than 0.5 arcsec. The plot shows the offset in right ascension (α) and declination (δ) of the VLBA position of the burst (see section 10.6) relative to the host center, $(\Delta\theta_{\rm RA}, \Delta\theta_\delta)$=(0,0). The most accurate measurements are at 8.46 GHz in the VLA A configuration. In this mode we achieved an rms positional error of 0.02 arcsec. The insert shows the weighted average offset in both α and δ (small cross). The larger cross is the offset measurement from Bloom et al. (2002a). The solid circle designates the projected maximum source size from the radio observations in the A configuration at 8.46 GHz, and the dashed circle is the optical size from Holland et al. (2001). Clearly the formation of massive stars is concentrated in the central region of the host. The small offset of the burst from the host center indicates that GRB 980703 occurred within the region of star formation, which points to a link between GRBs and massive stars.

IGM over a wide redshift range. In particular, radio and submillimeter/FIR observations of a GRB-selected galaxy sample will be extremely useful for the study of the obscured star formation fraction, and the properties of starbursts at high redshifts. Moreover, a comparison of the global star formation history as derived from these long-wavelength host studies, with the redshift distribution of GRBs, will provide valuable insight as to how well GRBs trace the formation rate of massive stars (e.g., Blain & Natarajan 2000); we expect that if GRBs trace only a particular channel of star formation, the two distributions will not agree.

Therefore, it is imperative to study the hosts of GRBs in the radio and submillimeter/FIR. Future observatories such as the Space Infrared Telescope Facility (SIRTF; to be launched in July 2002), the Atacama Large Millimeter Array (ALMA), the Expanded VLA (EVLA), and the Square-Kilometer Array (SKA) will allow detailed studies of these hosts. In the FIR, SIRTF will have the ability to detect sources down to several mJy, allowing the detection of galaxies with SFR comparable to that in the host of GRB 980703 out to $z \sim few$; alternatively, we will be able to detect hosts with SFR as low as a few tens of $M_\odot$/yr at $z \sim 1$. ALMA has a projected sensitivity ranging from a few μJy at 35 GHz to ~ 1 mJy at 850 GHz for a 10-minute observation, improving on the capability of an instrument such as

SCUBA by almost two orders of magnitude. Combined with an expected resolution of approximately 1 arcsec, ALMA will provide an unprecedented ability to study GRB host galaxies over a very wide redshift, SFR, and frequency range. The EVLA and SKA will greatly improve the detectability of host galaxies in the radio, and will also allow much higher angular resolution studies of compact star-forming regions. With a factor ten increase in resolution and a factor five increase in sensitivity over the current VLA, we will be able to probe scales of approximately 5 mas with the EVLA; for a galaxy at $z \approx 1$ this translates to a physical scale of 150 pc. In addition, EVLA will detect galaxies with a total SFR as low as 50 $M_\odot$/yr at $z \sim 1$. The SKA, with a similar resolution, but a much larger collecting area, will extend this capability to even lower SFR and smaller star-forming regions.

Thus, as more host galaxies are detected and studied in detail in the radio and submillimeter/FIR, we will be able to address a large number of issues pertaining not only to the bursts themselves, but also to the characteristics of galaxies at high redshifts.

We acknowledge support by NSF and NASA grants. SRK thanks Brian McBreen for useful comments on the ISO observations of GRB 970508.

Table 10.1. Late-time radio observations of GRB 980703

Epoch (UT)	Δt (days)	Config.	Time (hrs)	ν_0 (GHz)	S$\pm\sigma$ (μJy)	$\Delta\alpha$ (arcsec)	$\Delta\delta$ (arcsec)
1999 Jun. 15.36—26.29	352.65	A	6.5	1.43	81±18	-0.17 ± 0.17	0.03 ± 0.17
1999 Jul. 10.53—28.28	381.22	A	13.4	1.43	54±10	0.07 ± 0.09	-0.04 ± 0.09
1999 Aug. 19.40—Sep. 21.24	428.64	A	11.3	8.46	38±8	-0.06 ± 0.02	0.03 ± 0.02
1999 Nov. 24.06	508.88	B	1.7	1.43	72±11	0.01 ± 0.03	-0.03 ± 0.03
2000 Mar. 5.70	610.52	BnC	2.8	8.46	55±19	-0.16 ± 0.18	-0.26 ± 0.18
2000 Oct. 7.30—Nov. 19.08	847.01	A	6.5	1.43	60±13	0.01 ± 0.13	-0.03 ± 0.13
2000 Dec. 2.19—4.97	882.60	A	4.9	4.86	35±11	-0.12 ± 0.08	0.02 ± 0.08
2000 Dec. 21.15—2001 Jan. 4.98	908.38	A	7.0	8.46	40±8	0.02 ± 0.03	0.03 ± 0.03
2001 Feb. 2.00—4.93	945.29	AnB	1.9	1.43	119±23	-0.65 ± 0.30	-0.23 ± 0.30
2001 Feb. 8.08	949.90	AnB	1.2	4.86	67±28	1.22 ± 0.67	-0.38 ± 0.67
2001 Mar. 2.98—9.00	975.81	B	4.5	4.86	49±16	-1.21 ± 0.49	0.02 ± 0.49
2001 Mar. 13.97–17.98	985.80	B	4.5	8.46	29±12	0.45 ± 0.43	0.02 ± 0.43
2001 Mar. 22.96—Apr. 8.56	1001.08	B	2.6	1.43	83±30	-1.26 ± 1.76	-1.23 ± 1.76

Note. — The columns are (left to right), (1) UT date of the start of each observation or range of dates for observations which were added over several days, (2) time elapsed since the γ-ray burst, (3) array configuration, (4) total on-source observing time, (5) observing frequency, (6) peak flux density at the best fit position of the radio transient, with the error given as the root mean square noise on the image, (7) projected angular offset in RA between the host center and the position of GRB 980703, and (8) projected angular offset in declination.

CHAPTER 11

A Submillimeter and Radio Survey of Gamma-Ray Burst Host Galaxies: A Glimpse into the Future of Star Formation Studies†

E. Berger[a], L. L. Cowie[b], S. R. Kulkarni[a], D. A. Frail[c], H. Aussel[b] & A. J. Barger[b,d,e]

[a]Department of Astronomy, 105-24 California Institute of Technology, Pasadena, CA 91125, USA

[b]Institute for Astronomy, University of Hawaii, 2680 Woodlawn Drive, Honolulu, HI 96822

[c]National Radio Astronomy Observatory, P. O. Box 0, Socorro, NM 87801

[d]Department of Astronomy, University of Wisconsin-Madison, 475 North Charter Street, Madison, WI 53706

[e]Department of Physics and Astronomy, University of Hawaii, 2505 Correa Road, Honolulu, HI 96822

Abstract

We present the first comprehensive search for submillimeter and radio emission from the host galaxies of twenty well-localized γ-ray bursts (GRBs). With the exception of a single source, all observations were undertaken months to years after the GRB explosions to ensure negligible contamination from the afterglows. We detect the host galaxy of GRB 000418 in both the submillimeter and radio, and the host galaxy of GRB 000210 only in the submillimeter. These observations, in conjunction with the previous detections of the host galaxies of GRB 980703 and GRB 010222, indicate that about 20% of GRB host galaxies are ultra-luminous ($L > 10^{12}$ $L_\odot$) and have star formation rates of about 500 $M_\odot$ yr^{-1}. As an ensemble, the non-detected hosts have a star formation rate of about 100 $M_\odot$ yr^{-1} (5σ) based on their radio emission. This, in conjunction with an average luminosity for the entire sample that is approximately 20% fainter than the local starburst galaxy Arp 220, indicates that GRB hosts probe a more representative population of star forming galaxies than those uncovered in blank submillimeter and radio surveys. The detected and ensemble star formation rates exceed the values determined from various optical estimators by an order of magnitude, indicating significant dust obscuration. In the same vein, the ratio of bolometric dust luminosity to UV luminosity for the hosts detected in the submillimeter and radio ranges from about $\sim 30 - 500$, and follows the known trend of increasing obscuration with increasing bolometric luminosity. We also show that the GRB host sample as a whole and the submillimeter and radio detected hosts individually, have significantly bluer $R - K$ colors as

† A version of this chapter was published in *The Astrophysical Journal*, vol. 588, 99–112, (2003).

compared with galaxies selected in the submillimeter and radio in the same redshift range. This possibly indicates that the stellar populations in the GRB hosts are on average younger, supporting the massive stellar progenitor scenario for GRBs, but it is also possible that GRB hosts are on average less dusty. For the non-detected GRB hosts the difference in $R-K$ color may also be a manifestation of their more representative bolometric luminosities relative to the highly luminous submillimeter and radio selected galaxies. Beyond the specific results presented in this paper, the submillimeter and radio observations serve as an observational proof-of-concept in anticipation of the upcoming launch of the SWIFT GRB mission and SIRTF. These new facilities will possibly bring GRB host galaxies into the forefront of star formation studies.

SECTION 11.1

Introduction

One of the major thrusts in modern cosmology is an accurate census of star formation and star-forming galaxies in the Universe. This endeavor forms the backbone for a slew of methods (observational, analytical, and numerical) to study the process of galaxy formation and evolution over cosmic time. To date, star-forming galaxies have been selected and studied mainly in two observational windows: the rest-frame ultraviolet (UV), and rest-frame radio and far-infrared (FIR). For galaxies at high redshift these bands are shifted into the optical and radio/submillimeter, allowing observations from the ground. Still, the problem of translating the observed emission to star formation rate (SFR) involves large uncertainty. This is partly because each band traces only a minor portion of the total energy output of stars. Moreover, the optical/UV band is significantly affected by dust obscuration, thus requiring order of magnitude corrections, while the submillimeter and radio bands lack sensitivity, and therefore uncover only the most prodigiously star-forming galaxies.

The main result that has emerged from star formation surveys over the past few years is exemplified in the so-called Madau diagram. Namely, the SFR volume density, $\rho_{\rm SFR}(z)$, rises steeply to $z\sim 1$ (Lilly et al. 1996), and seemingly peaks at $z\sim 1-2$. There is still some debate about the how steep the rise is, with values ranging from $(1+z)^{1.5}$ (Wilson et al. 2002) to $(1+z)^4$ (e.g., Madau et al. 1996). The evolution beyond $z\sim 2$ is even less clear since optical/UV observations indicate a decline (Madau et al. 1996), while recent submillimeter observations argue for a flat $\rho_{\rm SFR}(z)$ to higher redshift, $z\sim 4$ (Barger et al. 2000). Consistency with this trend can be obtained by invoking large dust corrections in the optical/UV (Steidel et al. 1999). For general reviews of star formation surveys we refer the reader to Kennicutt (1998), Adelberger & Steidel (2000), and Blain et al. (2002).

Despite the significant progress in this field, our current understanding of star formation and its redshift evolution is still limited by the biases and shortcomings of current optical/UV, submillimeter, and radio selection techniques. In particular, despite the fact that the optical/UV band is sensitive to galaxies with modest star formation rates (down to a fraction of a $M_\odot$ yr^{-1}) at high redshift, these surveys may miss the most dusty, and vigorously star-forming galaxies. Moreover, it is not clear if the simple, locally-calibrated, prescriptions for correcting the observed *un-obscured* SFR for dust extinction (e.g., Meurer et al. 1999), hold at high redshift; even if they do, these prescriptions involve an order of magnitude correction above and beyond the inherent uncertainty in the conversion factors. Finally, the optical/UV surveys are magnitude limited, and therefore miss the faintest sources.

Submillimeter surveys have uncovered a population of highly dust-extincted galaxies, which are usually optically faint, and have star formation rates of several hundred $M_\odot$ yr^{-1} (e.g., Smail et al. 1997). However, unlike optical/UV surveys, submillimeter surveys are severely sensitivity limited, and only detect galaxies with $L_{\rm bol}\gtrsim 10^{12}$ $L_\odot$. More importantly, current submillimeter bolometer arrays (such as SCUBA) have large beams on the sky ($\sim$ 15 arcsec) making it difficult to unambiguously identify optical counterparts (which are usually faint to begin with), and hence measure the redshifts (Smail et al. 2002); in fact, of the $\sim$ 200 submillimeter galaxies identified to date, only a handful have a measured redshift. Finally, translating the observed submillimeter emission to a SFR requires significant

assumptions about the temperature of the dust, and the dust emission spectrum (e.g., Blain et al. 2002).

Surveys at decimeter radio wavelengths also suffer from low sensitivity, but the high astrometric accuracy afforded by synthesis arrays such as the VLA allows a sub-arcsec localization of the radio-selected galaxies. As a result, it is easier to identify the optical counterparts of these sources. Recently, this approach has been used to pre-select sources for targeted submillimeter observations resulting in an increase in the submillimeter detection rate (Barger et al. 2000; Chapman et al. 2002a) and redshift determination (Chapman et al. 2003). However, this method is biased toward finding luminous (high SFR) sources since it requires an initial radio detection. An additional problem with radio, even more than with submillimeter, selection is contamination by active galactic nuclei (AGN). An examination of the X-ray properties of radio and submillimeter selected galaxies reveals that of the order of 20% can have a significant AGN component (Barger et al. 2001).

The most significant problem with current star formation studies, however, is that the link between the optical and submillimeter/radio samples is still not well understood. The Hubble Deep Field provides a clear illustration: the brightest submillimeter source does not appear to have an optical counterpart (Hughes et al. 1998), and only recently a detection has been claimed in the near-IR ($K \approx 23.5$ mag; Dunlop et al. 2002). Along the same line, submillimeter observations of the optically-selected Lyman break galaxies have resulted in very few detections (Chapman et al. 2000; Peacock et al. 2000; Chapman et al. 2002b), and even the brightest Lyman break galaxies appear to be faint in the submillimeter band (Baker et al. 2001). In addition, there is considerable diversity in the properties of optical counterparts to submillimeter sources, ranging from galaxies which are faint in both the optical and near-IR (NIR) to those which are bright in both bands (Ivison et al. 2000; Smail et al. 2002).

As a result of the unclear overlap, and the sensitivity and dust problems in the submillimeter and optical surveys, there is still strong disagreement about the fractions of global star formation in the optical and submillimeter/radio selected galaxies (e.g., Adelberger & Steidel 2000; Scott et al. 2002. It is therefore not clear if the majority of star formation takes place in ultra-luminous galaxies with very high star formation rates, or in the more abundant lower luminosity galaxies with star formation rates of a few $M_\odot$ yr^{-1}. Given the difficulty with redshift identification of submillimeter galaxies, the redshift distribution of dusty star forming galaxies remains highly uncertain.

One way to alleviate some of these problems is to study a sample of galaxies that is immune to the selection biases of current optical/UV and submillimeter/radio surveys, and which may draw a more representative sample of the underlying distribution of star-forming galaxies. The host galaxies of γ-ray bursts (GRBs) may provide one such sample.

The main advantages of the sample of GRB host galaxies are: (i) The galaxies are selected with no regard to their emission properties in any wavelength regime, (ii) the dust-penetrating power of the γ-ray emission results in a sample that is completely unbiased with respect to the global dust properties of the hosts, (iii) GRBs can be observed to very high redshifts with existing missions ($z \gtrsim 10$; Lamb & Reichart 2000), and as a result volume corrections for the star formation rates inferred from their hosts are trivial, (iv) the redshift of the galaxy can be determined via absorption spectroscopy of the optical afterglow, or X-ray spectroscopy allowing a redshift measurement of arbitrarily faint galaxies (the current record-holder is the host of GRB 990510 with $R = 28.5$ mag and $z = 1.619$; Vreeswijk et al. 2001b), and (v) since there is excellent circumstantial evidence linking GRBs to massive stars (e.g., Bloom et al. 2002a), the sample of GRB hosts may trace global star formation (Blain & Natarajan 2000).

Of course, the sample of GRB hosts is not immune from its own problems and potential biases. First, the sample is much smaller than the optical and submillimeter samples[1] (although the number of GRB hosts with a known redshift exceeds the number of submillimeter galaxies with a measured redshift). As a result, at the present it is not possible to assess the SFR density that is implied by GRB hosts, or its redshift evolution. Morever, despite the link between GRBs and massive stars, it is not clear

[1] Currently, the sample of GRB hosts numbers about 30 sources, and grows at a rate of about one per month. The upcoming SWIFT mission is expected to increase the rate to one per $2-3$ days.

whether GRB progenitors are truly representative of massive stars. In particular, a bias towards sub-solar metallicity for GRB progenitors (and hence their environments) has been discussed (MacFadyen & Woosley 1999; MacFadyen et al. 2001), but it appears that very massive stars (e.g., $M \gtrsim 35$ M$_\odot$) should produce black holes even at solar metallicity. The impact of metallicity on additional aspects of GRB formation (e.g., angular momentum, loss of hydrogen envelope) is not clear at present. Regardless of the exact details of these potential biases and problems, it is safe to conclude that GRB hosts provide a new perspective of global star formation, which is at least subject to a different set of systematic problems than the optical/UV and submillimeter approach.

To date, GRB host galaxies have mainly been studied in the optical and NIR bands. With the exception of one source (GRB 020124; Berger et al. 2002a), every GRB localized to a sub-arcsecond position has been associated with a star-forming galaxy (Bloom et al. 2002a). These galaxies range from $R \approx 22 - 29$ mag, have a median redshift, $\langle z \rangle \sim 1$, and are generally typical of star-forming galaxies at similar redshifts in terms of morphology and luminosity (Djorgovski et al. 2001b), with star formation rates from optical spectroscopy of $\sim 1 - 10$ M$_\odot$ yr^{-1}. At the same time, there are hints for higher than average ratios of [Ne III] 3869 to [O II] 3727, possibly indicating the presence of massive stars (Djorgovski et al. 2001b). Only two host galaxies have been detected so far in the radio (GRB 980703; Berger et al. 2001b) and submillimeter (GRB 010222; Frail et al. 2002).

Here we present submillimeter and radio observations of a sample of 20 GRB host galaxies, ranging in redshift from about 0.4 to 4.5 (§11.2); one of the 20 sources is detected with high significance in both the submillimeter and radio bands, and an additional source is detected in the submillimeter (§11.3). We compare the detected submillimeter and radio host galaxies to local and high-z ultra-luminous galaxies in §11.4, and derive the SFRs in §11.5. We then compare the inferred SFRs of the detected host galaxies, and the ensemble of undetected hosts, to optical estimates in §11.6. Finally, we compare the optical properties of the GRB host galaxies to those of submillimeter and radio selected star-forming galaxies (§11.7).

SECTION 11.2

Observations

11.2.1 Target Selection

At the time we conducted our survey, the sample of GRB host galaxies numbered 25, twenty of which had measured redshifts. These host galaxies were localized primarily based on optical afterglows, but also using the radio and X-ray afterglow emission. Of the 25 host galaxies we observed eight in both the radio and submillimeter, seven in the radio, and five in the submillimeter. The galaxies were drawn from the list of 25 hosts at random, constrained primarily by the availability of observing time. Thus, the sample presented here does not suffer from any obvious selection biases, with the exception of detectable afterglow emission in at least one band.

Submillimeter observations of GRB afterglows, and a small number of host galaxies have been undertaken in the past. Starting in 1997, Smith et al. (1999) and Smith et al. (2001) have searched for submillimeter emission from the afterglow of thirteen GRBs. While they did not detect any afterglow emission, these authors used their observations to place constraints on emission from eight host galaxies, with typical 1σ rms values of 1.2 mJy. Since these were target-of-opportunity observations, they were not always undertaken in favorable observing conditions.

More recently, Barnard et al. (2003) reported targeted submillimeter observations of the host galaxies of four optically-dark GRBs (i.e., GRBs lacking an optical afterglow). They focused on these particular sources since one explanation for the lack of optical emission is obscuration by dust, which presumably points to a dusty host. None of the hosts were detected, with the possible exception of GRB 000210 (see §11.3.4), leading the authors to conclude that the hosts of dark bursts are not necessarily heavily dust obscured.

Thus, the observations presented here provide the most comprehensive and bias-free search for submillimeter emission from GRB host galaxies, and the first comprehensive search for radio emission.

11.2.2 Submillimeter Observations

Observations in the submillimeter band were carried out using the Sub-millimeter Common User Bolometer Array (SCUBA; Holland et al. 1999) on the James Clerk Maxwell Telescope (JCMT[2]). We observed the positions of thirteen well-localized GRB afterglows with the long (850 μm) and short (450 μm) arrays. The observations, summarized in Table 11.1, were conducted in photometry mode with the standard nine-jiggle pattern using the central bolometer in each of the two arrays to observe the source. In the case of GRB 000301C we used an off-center bolometer in each array due to high noise levels in the central bolometer.

To account for variations in the sky brightness, we used a standard chopping of the secondary mirror between the on-source position and a position 60 arcsec away in azimuth, at a frequency of 7.8125 Hz. In addition, we used a two-position beam switch (nodding), in which the beam is moved off-source in each exposure to measure the sky. Measurements of the sky opacity (sky-dips) were taken approximately every two hours, and the focus and array noise were checked at least twice during each shift.

The pointing was checked approximately once per hour using several sources throughout each shift, and was generally found to vary by $\lesssim 3$ arcsec (i.e., less than one quarter of the beam size). All observations were performed in band 2 and 3 weather with $\tau_{225\,\mathrm{GHz}} \approx 0.05 - 0.12$.

The data were initially reduced with the SCUBA Data Reduction Facility (SURF) following the standard reduction procedure. The off-position pointings were subtracted from the on-position pointings to account for chopping and nodding of the telescope. Noisy bolometers were removed to facilitate a more accurate sky subtraction (see below), and the data were then flat-fielded to account for the small differences in bolometer response. Extinction correction was performed using a linear interpolation between skydips taken before and after each set of on-source scans.

In addition to the sky subtraction offered by the nodding and chopping, short-term sky contributions were subtracted by using all low-noise off-source bolometers (sky bolometers). This procedure takes advantage of the fact that the sky contribution is correlated across the array. As a result, the flux in the sky bolometers can be used to assess the sky contribution to the flux in the on-source bolometer. This procedure is especially crucial when observing weak sources, since the measured flux may be dominated by the sky. We implemented the sky subtraction using SURF and our own routine using MATLAB. We found that in general the SURF sky subtraction under-estimated the sky contribution, and as a result over-estimated the source fluxes; the discrepancy in fluxes varied from about 0.1 to 0.5 mJy. Since the discrepancies were not severe, and to maintain a conservative approach we used the results of our own analysis routine. For this purpose we calculated the median value of the two (three) outer rings of bolometers in the 850 μm (450 μm) array, after removing noisy bolometers (defined as those whose standard deviation over a whole scan deviated by more than 5σ from the median standard deviation of all sky bolometers).

Following the sky subtraction, we calculated the mean and standard deviation of the mean (SDOM) for each source in a given observing shift. Noisy data were eliminated in two ways. First, the data were binned into 25 equal time bins, and the SDOM was calculated step-wise, i.e., at each step the data from an additional bin were added and the mean and SDOM were re-calculated. In an ideal situation where the data quality remains approximately constant, the SDOM should progressively decrease as more data are accumulated. However, if the quality of the data worsens (due to deteriorating weather conditions for example) the SDOM will increase. We therefore removed time bins in which the SDOM increased. After applying this procedure, we recursively eliminated individual noisy data points using a sigma cutoff level based on the number of data points (Chauvenet's criterion; Taylor 1982) until the

[2] The JCMT is operated by the Joint Astronomy Centre on behalf of the Particle Physics and Astronomy Research Council of the UK, the Netherlands Organization for Scientific Research, and National Research Council of Canada

mean converged on a constant value. Typically, two or three iterations were required, with only a few data points rejected each time. For all sources only a few percent of the data were rejected by the two procedures.

Finally, flux conversion factors (FCFs) were applied to the resulting voltage measurements to convert the signal to Jy. Using photometry observations of Mars and Uranus, and/or secondary calibrators (OH 231.8+4.2, IRC+10216, and CRL 618), we found the FCF to vary between $180-205$ Jy/V at 850 μm, consistent with the typical value of 197 ± 13. At 450 μm, the FCFs varied between $250-450$ Jy/V.

11.2.3 Radio Observations

Very Large Array (VLA[3]): We observed 12 GRB afterglow positions with the VLA from April 2001 to February 2002. All sources were observed at 8.46 GHz in the standard continuum mode with 2×50 MHz bands. In addition, GRB 000418 was observed at 1.43 and 4.86 GHz, and GRB 0010222 was observed at 4.86 GHz. In Table 11.2 we provide a summary of the observations.

In principle, since the median spectrum of faint radio sources between 1.4 and 8.5 GHz is $F_\nu\propto\nu^{-0.6}$ (Fomalont et al. 2002), the ideal VLA frequency for our observations (taking into account the sensitivity at each frequency) is 1.43 GHz. However, we chose to observe primarily at 8.46 GHz for the following reason. The majority of our observations were taken in the BnC, C, CnD, and D configurations, in which the typical synthesized beam size is $\sim10-40$ arcsec at 1.43 GHz, compared to $\sim2-8$ arcsec at 8.46 GHz. The large synthesized beam at 1.43 GHz, combined with the larger field of view and higher intrinsic brightness of radio sources at this frequency, would result in a significant decrease in sensitivity due to source confusion. Thus, we were forced to observe at higher frequencies, in which the reduced confusion noise more than compensates for the typical steep spectrum. We chose 8.46 GHz rather than 4.86 GHz since the combination of 20% higher sensitivity and 60% lower confusion noise, provide a more significant impact than the typical 30% decrease in intrinsic brightness. The 1.43 GHz observations of GRB 000418 were undertaken in the A configuration, where confusion does not play a limiting role.

For flux calibration we used the extragalactic sources 3C 48 (J0137+331), 3C 147 (J0542+498), and 3C 286 (J1331+305), while the phases were monitored using calibrator sources within $\sim5^\circ$ of the survey sources.

We used the Astronomical Image Processing System (AIPS) for data reduction and analysis. For each source we co-added all the observations prior to producing an image, to increase the final signal-to-noise.

Australia Telescope Compact Array (ATCA[4]): We observed the positions of four GRB afterglows during April 2002, in the 6A configuration at 1344 and 1432 MHz. Using the 6-km baseline resulted in a significant decrease in confusion noise, thus allowing observations at the most advantageous frequencies. The observations are summarized in Table 11.2.

We used J1934−638 for flux calibration, while the phase was monitored using calibrator sources within $\sim5^\circ$ of the survey sources. The data were reduced and analyzed using the Multichannel Image Reconstruction, Image Analysis and Display (MIRIAD) package, and AIPS.

11.2.4 Optical Data

The photometric and spectroscopic optical/NIR data used in this paper (see §11.6 and §11.7) have been collected from the literature. Host galaxy optical and NIR magnitudes are given in the Vega magnitude system. In addition, the star formation rates obtained from various optical estimators are corrected for extinction within the host galaxy when an estimate of the extinction is available (e.g., using the Balmer decrement, Djorgovski et al. 1998).

[3] The VLA is operated by the National Radio Astronomy Observatory, a facility of the National Science Foundation operated under cooperative agreement by Associated Universities, Inc.

[4] The Australia Telescope is funded by the Commonwealth of Australia for operations as a National Facility managed by CSIRO.

SECTION 11.3

Results

The flux measurements at the position of each GRB are given in Tables 11.1 and 11.2, and are plotted in Figure 11.1. Of the 20 sources, only GRB 000418 was detected in both the radio and submillimeter with $S/N > 3$ (§11.3.1). One additional source, GRB 000210, is detected with $S/N > 3$ when combining our observations with those of Barnard et al. (2003). Two hosts have radio fluxes with $3 < S/N < 4$ (GRB 000301C and GRB 000926), but as we show below this is due in part to emission from the afterglow.

The typical 2σ thresholds are about 2 mJy, 20 μJy, and 70 μJy in the SCUBA, VLA, and ATCA observations, respectively. In Figure 11.1 we plot all sources with $S/N > 3$ as detections, and the rest as 2σ upper limits. In addition, for the sources observed with the ATCA we plot both the 1.4 GHz upper limits, and the inferred upper limits at 8.46 GHz assuming a typical radio spectrum, $F_\nu \propto \nu^{-0.6}$ (Fomalont et al. 2002).

One obvious source for the observed radio and submillimeter fluxes (other than the putative host galaxies) is emission from the afterglows. To assess the possibility that our observations are contaminated by flux from the afterglows we note that the observations have been undertaken at least a year after the GRB explosion[5] . On this timescale, the submillimeter emission from the afterglow is expected to be much lower than the detection threshold of our observations. In fact, the brightest submillimeter afterglows to date have only reached a flux of a few mJy (at 350 GHz), and typically exhibited a fading rate of $\sim t^{-1}$ after about one day following the burst (Smith et al. 1999; Berger et al. 2000; Smith et al. 2001; Frail et al. 2002; Yost et al. 2002). Thus, on the timescale of our observations, the expected submillimeter flux from the afterglows is only ~ 10 μJy, well below the detection threshold.

The radio emission from GRB afterglows is more long-lived, and hence posses a more serious problem. However, on the typical timescale of the radio observations the 8.46 GHz flux is expected to be at most a few μJy (e.g., Berger et al. 2000).

In the following sections we discuss the individual detections in the radio and submillimeter, and also provide an estimate for the radio emission from each afterglow.

11.3.1 GRB 000418

A source at the position of GRB 000418 is detected at four of the five observing frequencies with $S/N > 3$. The SCUBA source, which we designate SMM 12252+2006, has a flux density of $F_\nu(350\,\mathrm{GHz}) \approx 3.2 \pm 0.9$ mJy, and $F_\nu(670\,\mathrm{GHz}) \approx 41 \pm 19$ mJy. These values imply a spectral index, $\beta \approx 3.9^{+1.1}_{-1.3}$ ($F_\nu \propto \nu^\beta$), consistent with a thermal dust spectrum as expected if the emission is due to obscured star formation.

The radio source (VLA 122519.26+200611.1), is located at right ascension α(J2000)=$12^{\rm h}25^{\rm m}19.255^{\rm s}$, and declination δ(J2000)=$20^\circ 06' 11.10''$, with an uncertainty of 0.1 arcsec in both coordinates. This position is offset from the position of the radio afterglow of GRB 000418 (Berger et al. 2001) by $\Delta\alpha = -0.40 \pm 0.14$ arcsec and $\Delta\delta = -0.04 \pm 0.17$ arcsec (Figure 11.2). In comparison, the offset measured from Keck and *Hubble Space Telescope* images is smaller, $\Delta\alpha = -0.019 \pm 0.066$ arcsec and $\Delta\delta = 0.012 \pm 0.058$ arcsec.

VLA 122519.26+200611.1 has an observed spectral slope $\beta = -0.17 \pm 0.25$, flatter than the typical value for faint radio galaxies, $\beta \approx -0.6$ (Fomalont et al. 2002), and similar to the value measured for the host of GRB 980703 ($\beta \approx -0.32$; Berger et al. 2001b). The source appears to be slightly extended at 1.43 and 8.46 GHz, with a size of about 1 arcsec (8.8 kpc at $z = 1.119$).

The expected afterglow fluxes at 4.86 and 8.46 GHz at the time of our observations are about 5 and 10 μJy, respectively (Berger et al. 2001a). At 1.43 GHz the afterglow contribution is expected to be about 10 μJy based on the 4.86 GHz flux and the afterglow spectrum $F_\nu \propto \nu^{-0.65}$. Thus, despite the contribution from the afterglow, the radio detections of the host galaxy are still significant at better than

[5] The single exception is GRB 011211 for which SCUBA observations were taken $18 - 20$ days after the burst.

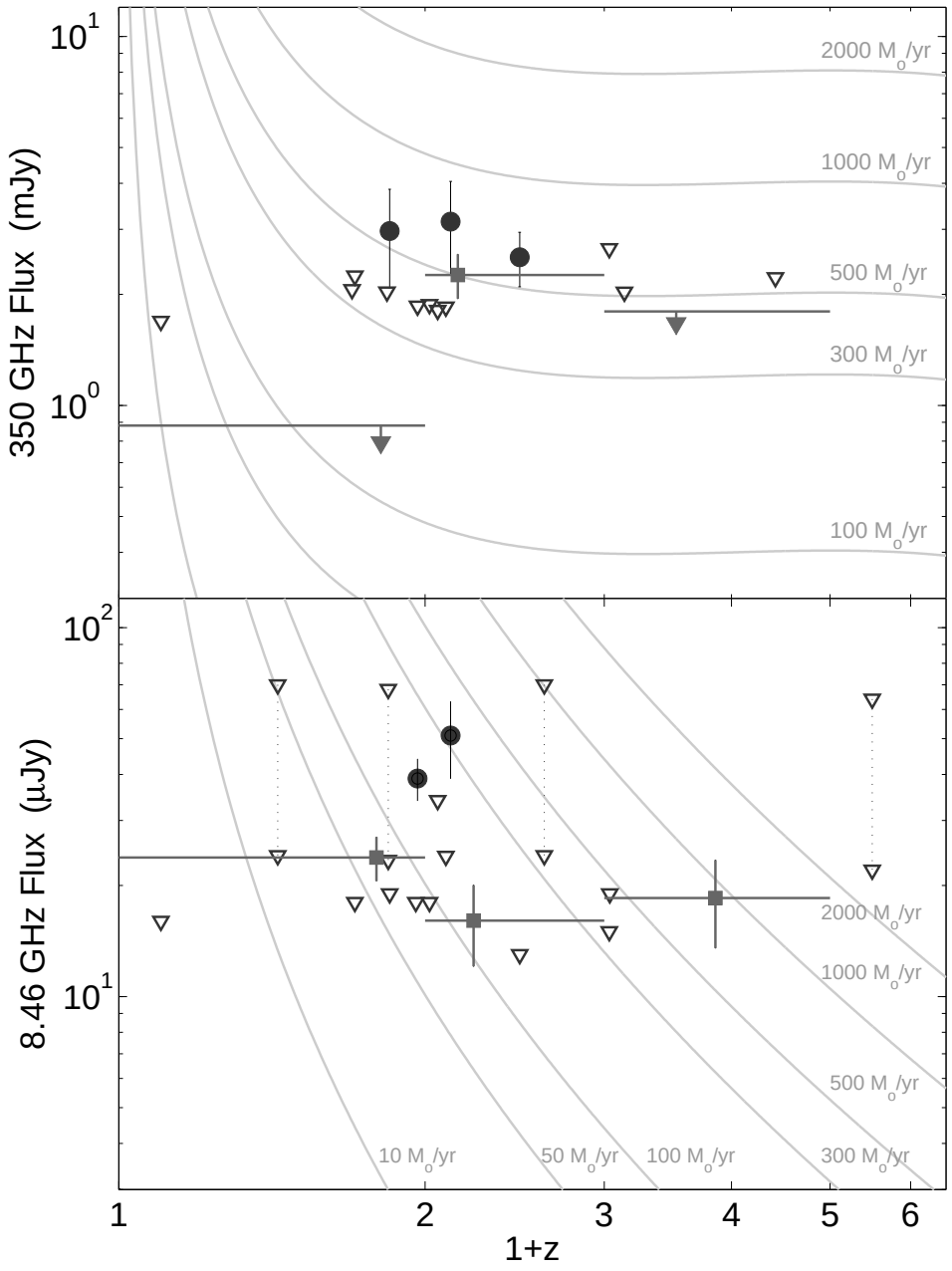

Figure 11.1: Submillimeter (top) and radio (bottom) fluxes for 20 GRB host galaxies plotted as a function of source redshift. The solid symbols are detections ($S/N > 2$ in the submillimeter and $S/N > 3$ in the radio), while the inverted triangles are 2σ upper limits. In the bottom panel, the upper limits linked by dotted lines are from the ATCA observations at 1.4 GHz (upper triangles) converted to 8.46 GHz (lower triangles) using $F_\nu \propto \nu^{-0.6}$. Also plotted are the ATCA upper limit for GRB 990712 ($z = 0.433$; Vreeswijk et al. 2001a), the VLA detection of the host of GRB 980703 (Berger et al. 2001b), and the submillimeter detection of the host of GRB 010222 Frail et al. (2002). The source at $1+z = 1.2$ in both panels is the host of GRB 980329 which does not have a measured redshift. The points and upper limits with horizontal error bars are weighted average fluxes in the redshift bins: $0 < z < 1$, $1 < z < 2$, and $z > 2$. Finally, the thin lines are contours of constant star formation rate (using Equation 11.1 with the parameters specified in §11.5).

3σ level. Correcting for the afterglow contribution we find an actual spectral slope $\beta = -0.29 \pm 0.33$, consistent with the median $\beta \approx -0.6$ for 8.46 GHz radio sources with a similar flux (Fomalont et al.

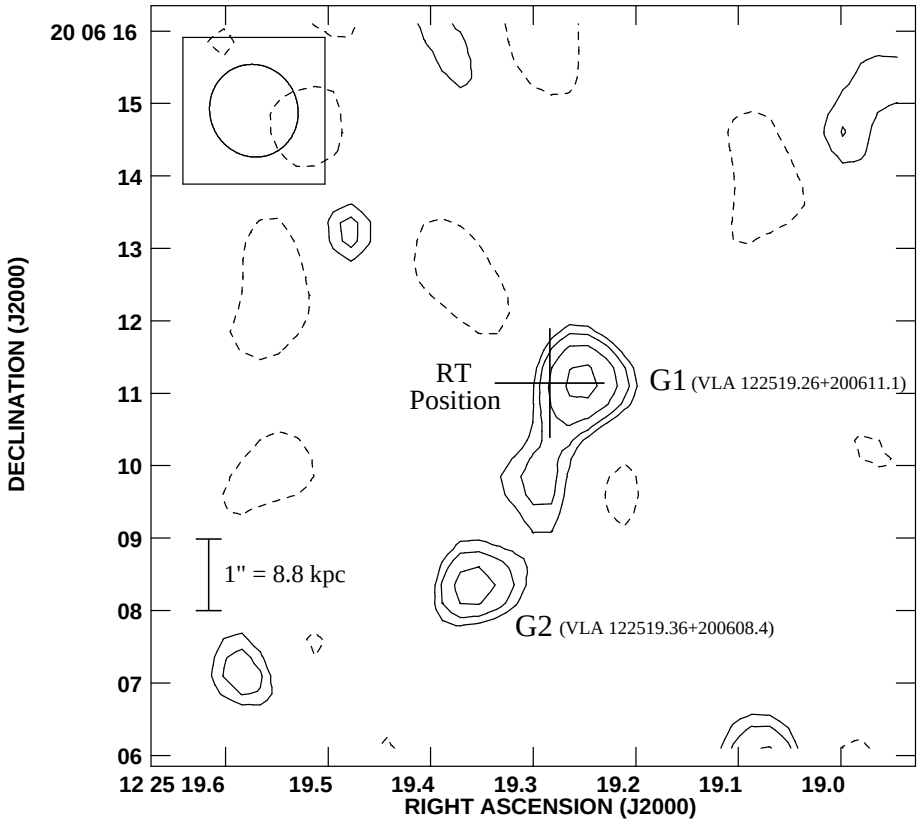

Figure 11.2: Contour plot of a 5×5 arcsec^2 field observed at 1.43 GHz and centered on the position (Berger et al. 2001b) of the radio transient associated with GRB 000418 (marked by cross). Contours are plooted at $-2^{1/2}, 2^{1/2}, 2^1, 2^{3/2}, 2^2$, and $2^{5/2}$. Source G1 is the host galaxy of GRB 000418, while source G2 is a possible companion galaxy. In addition, there appears to be a bridge of radio emission connecting galaxies G1 and G2. A comparison to the synthesized beam (upper left corner) reveals that G1 and G2 are slightly extended.

2002).

As with all SCUBA detections, source confusion arising from the large beam ($D_{\rm FWHM} \approx 14$ arcsec at 350 GHz and ≈ 6 arcsec at 670 GHz) raises the possibility that SMM 12252+2006 is not associated with the host galaxy of GRB 000418. Fortunately, the detection of the radio source, which is located 0.4 ± 0.1 arcsec away from the position of the radio afterglow of GRB 000418, indicates that SMM 12252+2006 and VLA 122519.26+200611.1 are in fact the same source — the host galaxy of GRB 000418.

Besides the positional coincidence of the VLA and SCUBA sources, we gain further confidence of the association based on the spectral index between the two bands, $\beta_{1.4}^{350}$. This spectral index is redshift dependent as a result of the different spectral slopes in the two regimes (Carilli & Yun 2000; Barger et al. 2000). We find $\beta_{1.4}^{350} \approx 0.73 \pm 0.10$, in good agreement with the Carilli & Yun (2000) value of $\beta_{1.4}^{350} = 0.59 \pm 0.16$ (for the redshift of GRB 000418, $z = 1.119$).

We also detect another source, slightly extended ($\theta \approx 1$ arcsec), approximately 1.4 arcsec East and 2.7 arcsec South of the host of GRB 000418 (designated VLA 122519.36+200608.4), with $F_\nu(1.43\,\mathrm{GHz}) = 48 \pm 15$ μJy and $F_\nu(8.46\,\mathrm{GHz}) = 37 \pm 12$ μJy (see Figure 11.2). This source appears to be linked by a bridge of radio emission (with $S/N \approx 1.5$ at both frequencies) to the host of GRB 000418. The physical separation between the two sources, assuming both are at the same redshift, $z = 1.119$, is 25 kpc. There is no obvious optical counterpart to this source in *Hubble Space Telescope* images down to about $R \sim 27.5$ mag.

Based purely on radio source counts at 8.46 GHz (Fomalont et al. 2002), the expected number of sources with $F_\nu(8.46\,\mathrm{GHz}) \approx 37$ μJy in a 3 arcsec radius circle is only about 2.7×10^{-4}. Thus, the coincidence of two such faint sources within 3 arcsec is highly suggestive of an interacting system, rather than chance superposition.

Interacting radio galaxies with separations of about 20 kpc, and joined by a bridge of radio continuum emission have been observed locally (Condon et al. 1993, 2002). In addition, optical surveys (e.g., Patton et al. 2002) show that a few percent of galaxies with an absolute B-band magnitude similar to that of the host of GRB 000418, have companions within about 30 kpc. The fraction of interacting systems is possibly much higher, $\sim 50\%$, in ultra-luminous systems (such as the host of GRB 000418), both locally (Sanders & Mirabel 1996) and at high redshift (e.g., Ivison et al. 2000).

We note that with a separation of only 3 arcsec, the host of GRB 000418 and the companion galaxy fall within the SCUBA beam. Thus, it is possible that SMM 12252+2006 is in fact a superposition of both radio sources. This will change the value of $\beta_{1.4}^{350}$ to about 0.46.

11.3.2 GRB 980703

The host galaxy of GRB 980703 has been detected in deep radio observations at 1.43, 4.86, and 8.46 GHz (Berger et al. 2001b). The galaxy has a flux $F_\nu(1.43\,\mathrm{GHz}) = 68.0 \pm 6.6$ μJy, and a radio spectral slope $\beta = -0.32 \pm 0.12$. In addition, the radio emission is unresolved with a maximum angular size of 0.27 arcsec (2.3 kpc).

Based on the Carilli & Yun (2000) value of $\beta_{1.4}^{350} \approx 0.54 \pm 0.16$ (for the redshift of GRB 980703, $z = 0.966$), the expected flux at 350 GHz is $F_\nu(350\,\mathrm{GHz}) \approx 1.3^{+1.9}_{-0.8}$ mJy. The observed (2σ) flux limit $F_\nu(350\,\mathrm{GHz}) < 1.8$ mJy, is consistent with the expected value.

11.3.3 GRB 010222

GRB 010222 has been detected in SCUBA and IRAM observations with a persistent flux of about 3.5 mJy at 350 GHz and 1 mJy at 250 GHz (Frail et al. 2002). The persistent emission, as well as the steep spectral slope, $\beta \approx 3.8$, indicated that while the detected emission was partially due to the afterglow of GRB 010222, it was dominated by the host galaxy. In fact, accounting for the expected afterglow emission, we find that the host galaxy has a flux, $F_\nu(350\,\mathrm{GHz}) \approx 2.5 \pm 0.4$ mJy.

The radio flux predicted from the submillimeter emission (Carilli & Yun 2000) is $F_\nu(1.43\,\mathrm{GHz}) \approx 55^{+80}_{-20}$ μJy (for $z = 1.477$, the redshift of GRB 010222), which corresponds to $F_\nu(4.86\,\mathrm{GHz}) \approx 15-60$ μJy, and $F_\nu(8.46\,\mathrm{GHz}) \approx 10-45$ μJy (assuming $\beta = -0.6$). Therefore, our measured values, $F_\nu(4.86\,\mathrm{GHz}) = 26 \pm 8$ μJy and $F_\nu(8.46\,\mathrm{GHz}) = 17 \pm 6$ μJy are consistent with the observed submillimeter emission.

The expected afterglow fluxes at 4.86 and 8.46 GHz are 3 and 4 μJy, respectively, significantly lower than the measured values. Thus, the observed flux mainly arises from the host.

11.3.4 GRB 000210

Recently, Barnard et al. (2003) measured a flux of 3.3 ± 1.5 mJy for GRB 000210, in good agreement with our value of 2.8 ± 1.1 mJy. A weighted average (here and elsewhere we use inverse-variance weighting) of the two measurements gives $F_\nu(350\,\mathrm{GHz}) = 3.0 \pm 0.9$ mJy, similar to the submillimeter flux from the host galaxies of GRB 000418 and GRB 010222. The radio flux at the position of GRB 000210 is

$F_\nu(8.46\,\mathrm{GHz}) = 18 \pm 9$ μJy. Based on a redshift of 0.846 (Piro et al. 2002) and the submillimeter detection, the expected radio flux from this source (Carilli & Yun 2000) is $F_\nu(8.46\,\mathrm{GHz}) \approx 10 - 50$ μJy, consistent with the measured value. The expected flux of the afterglow at the time of the radio observations is less than 1 μJy (Piro et al. 2002).

11.3.5 GRB 980329

Following the localization of GRB 980329, Smith et al. (1999) observed the afterglow position with SCUBA and claimed the detection of a source with a 350 GHz flux of about 5.0 ± 1.5 mJy on 1998, Apr. 5.2 UT. Subsequent observations indicated a fading trend, with a decline to 4.0 ± 1.2 mJy on Apr. 6.2, and < 1.8 mJy (2σ) on Apr. 11.2. Based on a comparison to the radio flux of the afterglow, Smith et al. (1999) concluded that the detected submillimeter flux was in excess of the emission from the afterglow itself, and therefore requires an additional component, most likely a host galaxy.

Recently, Yost et al. (2002) re-analyzed the SCUBA data and showed that the initial submillimeter flux was in fact only about 2.5 mJy, and perfectly consistent with the afterglow flux. As a result, it is not clear that an additional persistent component is required. We also re-analyzed the data from Apr. 1998 using the method described in §11.2.2. We find the following fluxes: 2.4 ± 1.0 mJy (Apr. 5), 2.4 ± 1.1 mJy (Apr. 6), 1.2 ± 0.8 mJy (Apr. 7), 1.4 ± 0.9 mJy (Apr. 8), and 1.6 ± 0.8 mJy (Apr. 11). A comparison to the results in Smith et al. (1999) reveals that, with the exception of the last epoch, they over-estimate the fluxes by about $0.5 - 2.5$ mJy.

Our observations of GRB 980329 from September and October of 2001 reveal a flux, $F_\nu(350\,\mathrm{GHz}) = 1.8 \pm 0.8$ mJy, indicating that the flattening to a value of about 1.5 mJy in the late epochs of the Apr. 1998 observations may indicate emission from the host galaxy.

The radio observations are similarly inconclusive, with $F_\nu(8.46\,\mathrm{GHz}) = 18 \pm 8$ μJy. We estimate that the flux of the afterglow at 8.46 GHz at the time of our observations is only $1 - 2$ μJy (Yost et al. 2002).

Since the redshift of GRB 980329 is not known, we cannot assess the expected ratio of the radio and submillimeter fluxes.

11.3.6 GRB 000926

This source is detected in the VLA observations with a flux of $F_\nu(8.46\,\mathrm{GHz}) = 33 \pm 9$ μJy (3.7σ). The expected flux from the afterglow at the time of the observations, ≈ 420 days after the burst, is 10 μJy (Harrison et al. 2001). Thus, the observed emission exceeds the afterglow flux by 2.6σ. In the calculations below we use a host flux of 23 ± 9 μJy.

11.3.7 GRB 000301C

The VLA observations of this GRB position reveal a source with $F_\nu(8.46\,\mathrm{GHz}) = 23 \pm 7$ μJy (3.1σ). The flux of the afterglow at the time of the observations is about 5 μJy (Berger et al. 2000). Thus, the excess emission is significant at the 2.5σ level.

The submillimeter emission predicted based on the Carilli & Yun (2000) relation is $F_\nu(350\,\mathrm{GHz}) = 1.5^{+3.7}_{-1.1}$ mJy (for $z = 2.034$, the redshift of GRB 000301C). This value is in agreement with the measured flux of -1 ± 1.3 mJy.

SECTION 11.4

Spectral Energy Distributions

In Figure 11.3 we plot the radio-to-UV spectral energy distributions (SEDs) of the detected host galaxies of GRB 980703, GRB 000418, and GRB 010222, as well as that of Arp 220, a proto-typical local ultra-luminous IR galaxy (ULIRG; Soifer et al. 1984), and ERO J164502+4626.4 (HuR 10), a high-z analog

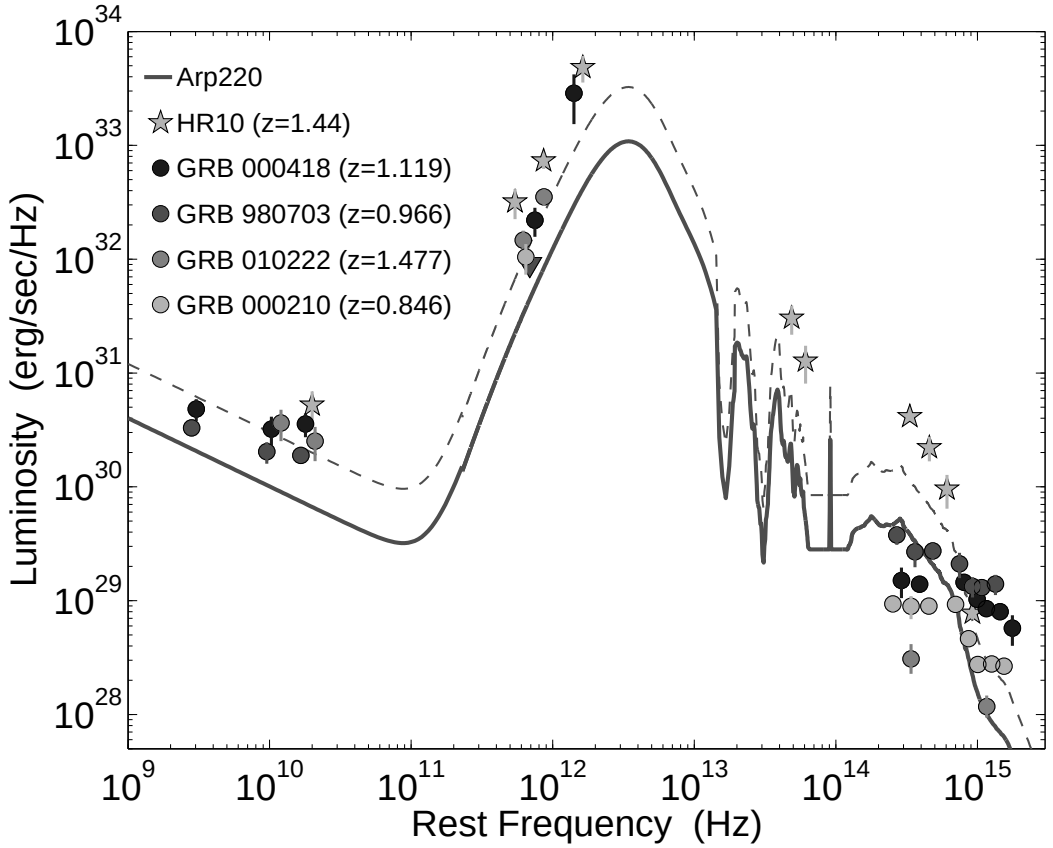

Figure 11.3: SEDs of the host galaxies of GRB 000418, GRB 980703, and GRB 010222 compared to the SED of the local starburst galaxy Arp 220, and the high-z starburst galaxy HuR 10. The luminosities are plotted at the rest frequencies to facilitate a direct comparison. The GRB host galaxies are more luminous than Arp 220, and are similar to HuR 10, indicating that their bolometric luminosities exceed 10^{12} $L_\odot$, and their star formation rates are of the order of 500 $M_\odot$ yr^{-1}. On the other hand, the spectral slopes in the optical regime are flatter than both Arp 220 and HuR 10, indicating that the GRB host galaxies are bluer than Arp 220 and HuR 10.

of Arp 220 (Hu & Ridgway 1994; Elbaz et al. 2002). The luminosities are plotted as a function of rest-frame frequencies, to facilitate a direct comparison.

The detected GRB hosts are somewhat brighter than Arp 220 ($L \approx 2 \times 10^{12}$ $L_\odot$, SFR$\approx$ 300 $M_\odot$ yr^{-1}), and are similar in luminosity to HuR 10 ($L \approx 7 \times 10^{12}$ $L_\odot$, SFR$\sim 10^3$ $M_\odot$ yr^{-1}; Dey et al. 1999). As such, we expect the host galaxies to have star formation rates of a few$\times$100 $M_\odot$ yr^{-1}, and bolometric luminosities in excess of 10^{12} $L_\odot$.

On the other hand, the average luminosity in the submillimeter band for all the observed hosts (detected and non-detected) is $\langle L_{\nu,s} \rangle \approx 2.1 \times 10^{31}$ erg s^{-1} Hz^{-1} at an effective rest-frame frequency of 7.9×10^{11} Hz, a factor of three less luminous than Arp 220. Similarly, in the radio band, at n effective frequency of 18 GHz, the average luminosity, $\langle L_{\nu,r} \rangle \approx 6.5 \times 10^{29}$ erg s^{-1} Hz^{-1}, is a factor of four less luminous than Arp 220.

In Figure 11.3 we use a more sophisticated approach to study the average SED of all GRB hosts in this survey, by scaling the SED of Arp 220 using a χ^2 statistic. We find that the average SED of GRB hosts in 20% fainter in both the submillimeter and radio bands than Arp 220. This clearly indicates that on average GRBs select galaxies that are less luminous than the typical submillimeter selected ULIRGs, and are therefore more representative of the general population of star-forming galaxies.

In the optical/NIR properties of the detected GRB hosts are distinctly different than those of Arp 220

and HuR 10 (as well as other local and high-z ULIRGs). In particular, from Figure 11.3 it is clear that, while the GRB host galaxies are similar to HuR 10 and Arp 220 in the radio and submillimeter bands, their optical/NIR colors (as defined for example by $R-K$) are much bluer. Moreover, while there is a dispersion of a factor of few in the radio and submillimeter bands between the GRB hosts, HuR 10, and Arp 220, the dispersion in the optical/NIR luminosity is about two orders of magnitude. This indicates that there is no simple correlation between the optical/NIR luminosities of GRB hosts (and possibly other galaxies, Adelberger & Steidel 2000) and their FIR and radio luminosities. In the following sections we expound on both points.

SECTION 11.5

Star Formation Rates

To evaluate the star formation rates that are implied by the submillimeter and radio measurements, we use the following expression for the observed flux as a function of SFR (Yun & Carilli 2002):

$$F_\nu(\nu_{\rm obs}) = \left(25 f_{\rm nth}\nu_0^{-\beta} + 0.71\nu_0^{-0.1} + 1.3\times10^{-6}\nu_0^3\frac{1-\exp[-(\nu_0/2000)^{1.35}]}{\exp(0.00083\nu_0)-1}\right)\frac{(1+z){\rm SFR}}{d_L^2}\ {\rm Jy}. \quad (11.1)$$

Here, $\nu_0 = (1+z)\nu_{\rm obs}$ GHz, SFR is the star formation rate in $M_\odot$ yr^{-1}, d_L is the luminosity distance in Mpc, and $f_{\rm nth}$ is a scaling factor (of order unity) which accounts for the difference in the conversion between synchrotron flux and SFR in the Milky Way and other galaxies. The first term on the right-hand-side accounts for the fact that non-thermal synchrotron emission arising from supernova remnants is proportional to the SFR, while the second term is the contribution of free-free emission from HII regions. These two flux terms dominate in the radio regime.

The last term in Equation. 11.1 is the dust spectrum, which dominates in the submillimeter and FIR regimes. In this case, the parameters that have been chosen to characterize the spectrum are a dust temperature, $T_d = 58$ K, and a dust emissivity, $\beta = 1.35$, based on a sample of 23 IR-selected starburst galaxies with $L_{\rm FIR} > 10^{11}$ $L_\odot$ (Yun & Carilli 2002). We note that other authors (e.g., Blain et al. 2002) favor a lower dust temperature, $T_d \approx 40$ K, which would result in star formation rates that are higher by about 70%.

To calculate d_L we use the cosmological parameters $\Omega_{\rm m} = 0.3$, $\Omega_\Lambda = 0.7$, and $H_0 = 65$ km s^{-1} Mpc^{-1}. We also use the typical value $\beta \approx -0.6$ for the radio measurements (Fomalont et al. 2002). In Figure 11.1 we plot contours of constant SFR overlaid on the submillimeter and radio flux measurements. Our radio observations are sensitive to galaxies with SFR > 100 $M_\odot$ yr^{-1} at $z \sim 1$, and SFR > 1000 $M_\odot$ yr^{-1} at $z \sim 3$. The submillimeter flux, on the other hand, is relatively constant for a given SFR, independent of z. This is due to the large positive k-correction resulting from the steep thermal dust spectrum. Therefore, at the typical limit of our submillimeter observations we are sensitive to galaxies with SFR$\gtrsim 500$ $M_\odot$ yr^{-1}.

For the host galaxies that are detected with $S/N > 3$ in the submillimeter and radio, as well as those detected in the past (i.e., GRB 980703 and GRB 010222) we calculate the following star formation rates: GRB 000418 – SFR$_S = 690\pm200$ $M_\odot$ yr^{-1}, SFR$_R = 330\pm75$ $M_\odot$ yr^{-1}; GRB 000210 – SFR$_S = 560\pm170$ $M_\odot$ yr^{-1}; GRB 010222 – SFR$_S = 610\pm100$ $M_\odot$; GRB 980703 – SFR$_R = 180\pm25$ $M_\odot$ yr^{-1}. Here SFR$_S$ and SFR$_R$ are the SFRs derived from the submillimeter and radio fluxes, respectively. We note that the difference in the radio and submillimeter derived SFRs for GRB 000418 are an indication of the uncertainty in the dust properties and the parameter $f_{\rm nth}$.

The detections and upper limits from this survey, combined with the detections and upper limits discussed in the literature (Berger et al. 2001b; Vreeswijk et al. 2001a; Frail et al. 2002) indicate that about 20% of all GRBs explode in galaxies with star formation rates of few $\times 100$ $M_\odot$ yr^{-1}. A similar conclusion has been reached from the shape of the 850 μm background (Barger et al. 1999). At the same time, it is clear that $\sim 80\%$ of GRB host galaxies have more modest star formation rates, SFR $\lesssim 100$

$M_\odot$ yr^{-1}.

Despite the fact that the majority of the survey sources are not detected, we can ask the question of whether the GRB host galaxies exhibit a significant submillimeter and/or radio emission *on average*. The weighted average emission from the non-detected sources ($S/N < 3$) is $\langle F_\nu(350\,\mathrm{GHz})\rangle = 0.37 \pm 0.34$ mJy, and $\langle F_\nu(8.46\,\mathrm{GHz})\rangle = 17.1 \pm 2.7$ μJy. This average radio flux is possibly contaminated by flux from the afterglows at the level of about 3 μJy, so we use $\langle F_\nu(8.46\,\mathrm{GHz})\rangle \approx 14 \pm 2.7$ μJy (5.2σ). Therefore, as an ensemble, the GRB host galaxies exhibit radio emission, but no significant submillimeter emission. Using the median redshift, $z \approx 1$, for the non-detected sample, the average radio flux implies an average $\langle \mathrm{SFR_R}\rangle \approx 100$ $M_\odot$ yr^{-1}, while the submillimeter 2σ upper limit on $\langle \mathrm{SFR_S}\rangle$ is about 150 $M_\odot$ yr^{-1}.

The average submillimeter flux can be compared to $\langle F_\nu(350\,\mathrm{GHz})\rangle = 0.8 \pm 0.3$ mJy for the non-detected submillimeter sources in a sample of radio pre-selected, optically faint ($I > 25$ mag) galaxies (Chapman et al. 2001), $\langle F_\nu(350\,\mathrm{GHz})\rangle = 0.4 \pm 0.2$ mJy for Lyman break galaxies (Webb et al. 2003), or $\langle F_\nu(350\,\mathrm{GHz})\rangle \approx 0.2$ mJy for optically-selected starbursts in the Hubble Deep Field (Peacock et al. 2000). Thus, it appears that GRB host galaxies trace a somewhat fainter population of submillimeter galaxies compared to the radio pre-selected sample, but similar to the Lyman break and HDF samples. This is not surprising given that the radio pre-selection is naturally biased in favor of luminous sources.

We can further extend this analysis by calculating the average submillimeter and radio fluxes in several redshift bins. Here we include both detections and upper limits. From the submillimeter (radio) observations we find: $\langle F_\nu\rangle = -0.2 \pm 0.4$ mJy ($\langle F_\nu\rangle = 24 \pm 3$ μJy) for $z = 0-1$, $\langle F_\nu\rangle = 2.3 \pm 0.3$ mJy ($\langle F_\nu\rangle = 16 \pm 4$ μJy) for $z = 1-2$, and $\langle F_\nu\rangle = 0.5 \pm 0.7$ mJy ($\langle F_\nu\rangle = 18 \pm 5$ μJy) for $z > 2$. These average fluxes are marked in Figure 11.1. In the submillimeter there is a clear increase in the average flux from $z < 1$ to $z \sim 1-2$, and a flattening or decrease beyond $z \sim 2$. In the radio, on the other hand, The average flux is about the same in all three redshift bins.

The average radio fluxes translate into the following star formation rates: for $z < 1$ the inferred average SFR is ~ 110 $M_\odot$ yr^{-1}, for $1 < z < 2$ it is ~ 200 $M_\odot$ yr^{-1}, and for $z > 2$ it is ~ 700 $M_\odot$ yr^{-1} (with $> 3\sigma$ significance in each bin). The submillimeter observations on the other hand, indicate a rise from a value of $\lesssim 160$ $M_\odot$ yr^{-1} for $z < 1$ to ~ 510 $M_\odot$ yr^{-1} for $1 < z < 2$, followed by a decline to $\lesssim 320$ $M_\odot$ yr^{-1} for $z > 2$. The difference between the two sets of SFR estimates is probably a combination of the stronger redshift dependence in the radio band, and the inherent uncertainties in the conversion factors (e.g., dust properties).

SECTION 11.6

Comparison to Optical Observations

The typical *un-obscured* star formation rates inferred from optical spectroscopy (i.e., using the UV continuum, recombination lines, and forbidden lines) are of the order of $1-10$ $M_\odot$ yr^{-1} (e.g., Djorgovski et al. 2001b). In particular, the host galaxy of GRB 980703 has an optical SFR of about 10 $M_\odot$ yr^{-1} (Djorgovski et al. 1998), compared to about 180 $M_\odot$ yr^{-1} from the radio observations. Similarly, the host of GRB 000418 has an optical SFR of about 55 $M_\odot$ yr^{-1} (Bloom et al. 2003a), compared to about $300-700$ $M_\odot$ yr^{-1} based on the radio and submillimeter detections, while the host of GRB 000210 has an optical SFR of ~ 3 $M_\odot$ yr^{-1} compared to about 550 $M_\odot$ yr^{-1} from the submillimeter observations. Finally, the average radio SFR for the non-detected sources, ~ 100 $M_\odot$ yr^{-1}, significantly exceeds the average optical SFR.

The discrepancy between the optical and radio/submillimeter star formation rates indicates that the majority of the star formation in the GRB host galaxies that are detected in the submillimeter and radio is obscured by dust. It is possible that the same is true for the sample as a whole, but this relies on the less secure average SFR in the non-detected hosts. The significant dust obscuration is not surprising given that a similar trend has been noted in high-z starburst galaxies, for which the typical dust corrections (based on the UV slope technique) are an order of magnitude (Meurer et al. 1999). In this case we find similar correction factors.

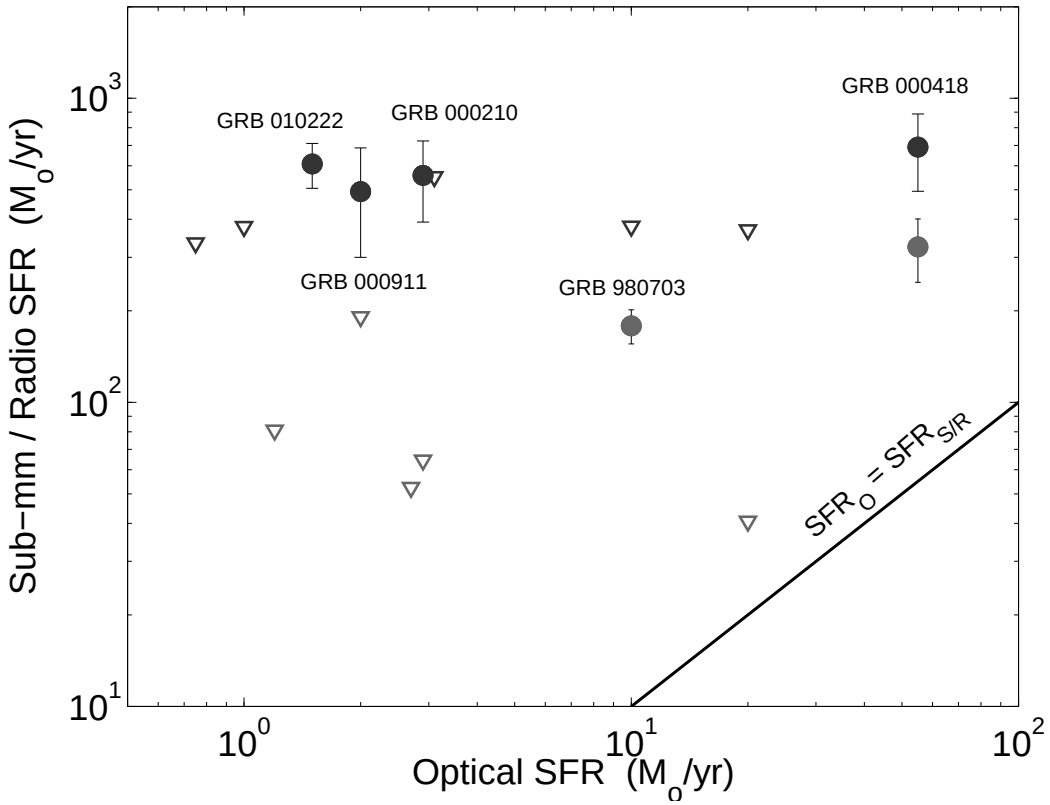

Figure 11.4: Submillimeter/radio vs. optical (i.e., from luminosity of UV continuum, recombination lines, and forbidden lines) star formation rates for several GRB host galaxies. The line in the bottom right corner designates a one-to-one correspondence between the two SFRs. Clearly, the hosts that gave appreciable submillimeter and/or radio flux have a large fraction of obscured star formation. In fact, the GRB hosts with a higher dust bolometric luminosity have a higher fraction of obscured star formation.

We can also assess the level of obscuration by comparing the UV luminosity at 1600Å, L_{1600}, to the bolometric dust luminosity, $L_{\rm bol,dust}$. The ratio of these two quantities provides a rough measure of the obscuration, while the sum provides a rough measure of the total star formation rate (Adelberger & Steidel 2000). To estimate L_{1600} we use the following host magnitudes: $B \approx 23.2$ mag (GRB 980703; Bloom et al. 1998a), $U \approx 23.5$ mag (GRB 0000210; Gorosabel et al. 2002), $R \approx 23.6$ mag (GRB 000418; Berger et al. 2001a), and $B \approx 26.7$ mag (GRB 010222; Frail et al. 2002). We extrapolate to rest-frame 1600Å using the mean value of $\langle U - R \rangle \approx 0.8$ mag found for Balmer-break galaxies, and $\langle U - R \rangle \approx 1.6$ mag found for $z \sim 1$ galaxies in the HDF that have the largest values of $L_{\rm bol,dust}$. These colors correspond to spectral slopes of -2.4 and -3.8, respectively. The resulting values of L_{1600} are: $(3.4 - 5.2) \times 10^{10}$ $L_\odot$ (GRB 980703), $(3.1 - 4.0) \times 10^{10}$ $L_\odot$ (GRB 000210), $(0.8 - 1.8) \times 10^{10}$ $L_\odot$ (GRB 000418), and $(0.9 - 1.0) \times 10^{10}$ $L_\odot$ (GRB 010222); the lower values are for $\beta = -3.8$. The mean values of L_{1600}, with the uncertainty defined as a combination of the range of reasonable spectral slopes and the intrinsic uncertainty in the host magnitudes are plotted in Figure 11.5.

We estimate $L_{\rm bol,dust}$ from the submillimeter fluxes (with the exception of GRB 980703 for which we use the radio flux) using the conversion factors given in equations 2 and 5 of Adelberger & Steidel (2000). The resulting values are: 1.3×10^{12} $L_\odot$ (GRB 980703), 3.3×10^{12} $L_\odot$ (GRB 000210), 4.4×10^{12} $L_\odot$ (GRB 000418), and 4.1×10^{12} $L_\odot$ (GRB 010222). Thus, $L_{\rm bol,dust}/L_{1600}$ evaluates to: $25 - 40$ (GRB 980703), $80 - 105$ (GRB 000210), $245 - 550$ (GRB 000418), and $410 - 455$ (GRB 010222). These results, as well as the sample of starbursts and ULIRGs at $z \sim 1$ taken from Adelberger & Steidel (2000) are plotted in Figure 11.5. We note that the GRB hosts are within the scatter of the $z \sim 1$

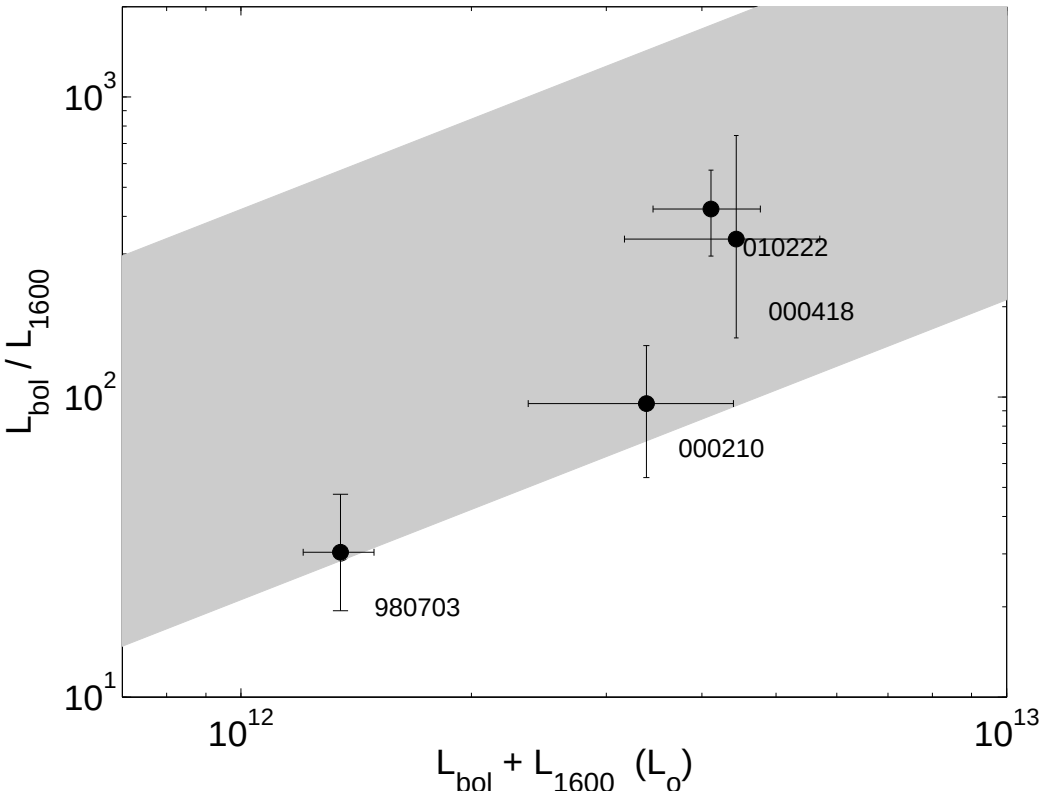

Figure 11.5: Ratio of bolometric luminosity, $L_{\rm bol}$ to luminosity at 1600 Å, L_{1600} plotted as a function of the combined luminosity. The ordinate provides a measure of the amount of dust obscuration, while the abscissa provides a measure of the total star formation rate. Black circles are the host galaxies detected here and by Berger et al. (2001b) and Frail et al. (2002), while the shaded region is from Adelberger & Steidel (2000) based on observations of starbursts and ULIRGs at $z \sim 1$. Clearly, there is a trend in both samples for more dust obscuration at higher star formation rates.

sample, following the general trend of increasing value of $L_{\rm bol,dust}/L_{1600}$ (i.e., inceasing obscuration) with increasing $L_{\rm bol,dust} + L_{1600}$ (i.e., inceasing SFR).

At the same time, the particular lines of sight to the GRBs within the submillimeter/radio bright host galaxies do not appear to be heavily obscured. For example, an extinction of $A_V^{\rm host} \sim 1$ mag has been inferred for GRB 980703 (Frail et al. 2003b), $A_V^{\rm host} \sim 0.4$ mag has been found for GRB 000418 (Berger et al. 2001a), and $A_V^{\rm host} \sim 0.1$ mag has been found for GRB 010222. The optically-dark GRB 000210 suffered more significant extinction, $A_R^{\rm host} > 1.6$ mag. In addition, the small offset of GRB 980703 relative to its radio host galaxy (0.04 arcsec; 0.3 kpc at the redshift of the burst), combined with the negligible extinction, indicates that while the burst probably exploded in a region of intense star formation, it either managed to destroy a large amount of dust in its vicinity, or the dust distribution is patchy. It is beyond the scope of this paper to evaluate the potential of dust destruction by GRBs (see e.g., Waxman & Draine 2000), but it is clear that the GRBs that exploded in the detected submillimeter and radio host galaxies, did not occur in the most heavily obscured star formation sites.

SECTION 11.7

Comparison of the Optical/NIR Colors of GRB hosts to Radio and Submillimeter Selected Galaxies

As we noted in §11.4, the optical/NIR colors of the detected GRB host galaxies are bluer than those of Arp 220 ($R - K \approx 4$ mag) and HuR 10 ($I - J \approx 5.8$ mag; Dey et al. 1999). In this section we compare

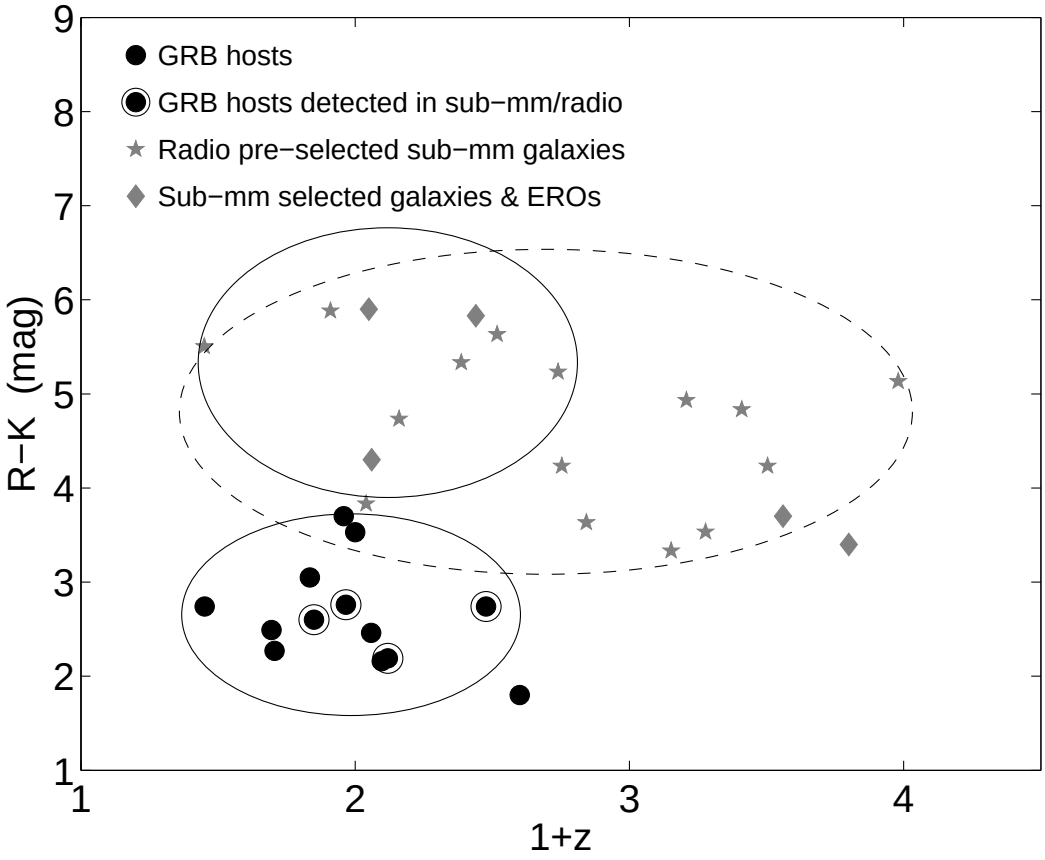

Figure 11.6: $R-K$ color as a function of redshift for GRB host galaxies, and radio pre-selected submillimeter selected (Chapman et al. 2003). The solid ellipses are centered on the mean color and redshift for each population of galaxies in the redshift range $z < 1.6$, and have widths of 2σ. The dashed ellipse is the same for the submillimeter population as a whole. Clearly, the GRB hosts are significantly bluer than the submillimeter galaxies in the same redshift range, indicating a possible preference for younger star formation episodes in GRB selected galaxies.

the $R-K$ color of GRB hosts to the $R-K$ colors of radio pre-selected submillimeter galaxies (Chapman et al. 2003) and submillimeter selected galaxies with a known optical counterpart and a redshift (Frayer et al. 1998; Ivison et al. 1998; Frayer et al. 1999).

In Figure 11.6 we plot $R-K$ color versus redshift for GRB hosts and radio pre-selected submillimeter galaxies. The optical and NIR data are collected from the literature, and are given in the Vega magnitudes. Before comparing the two populations, we note that the mean $R-K$ color and redshift for the entire GRB sample are 2.6 ± 0.6 mag and 1.0 ± 0.3, respectively, and for the hosts that are detected in the submillimeter and radio they are 2.6 ± 0.3 mag and 1.1 ± 0.3, respectively. Thus, there is no clear correlation between the optical/NIR colors of the GRB hosts and their submillimeter/radio luminosity.

For the sample of radio pre-selected and submillimeter selected galaxies the mean $R-K$ color and redshift are 4.6 ± 1.0 mag and 1.8 ± 0.7, respectively. To facilitate a more direct comparison with the GRB sample we also calculate the mean values for the same redshift range as the GRB hosts: $\langle R-K \rangle = 5.1 \pm 0.9$ mag and $\langle z \rangle = 1.1 \pm 0.3$. Clearly, the GRB host galaxies are on average significantly bluer than galaxies selected in the radio and submillimeter in the same redshift range.

Moreover, if we examine only the host galaxies that were detected in the radio and submillimeter with high significance we find $R-K$ colors of: 2.2 mag (GRB 000418), 2.8 mag (GRB 980703), 2.1 mag (GRB 010222), and 2.6 (GRB 000210). The bluest submillimeter and radio selected galaxies, on the other hand, have $R-K \approx 3.1$ mag.

The obvious difference in $R-K$ color indicates that the GRB and radio/submillimeter selections result in a somewhat different set of galaxies. The red colors of the submillimeter selected galaxies are not surprising since these sources are expected to be dust obscured. On the other hand, the mean color of the GRB hosts is bluer by about 2.5 mag (2.3σ significance) compared to submillimeter galaxies in the same redshift range, indicating a bias towards less dust obscuration. a more patchy dust distribution, or intrinsically bluer colors.

It is possible that there is a bias toward less dust obscuration in the general GRB host sample because the bursts that explode in dusty galaxies would have obscured optical afterglows, and hence no accurate localization. However, this is not a likely explanation since the GRBs which exploded in the submillimeter and radio bright hosts are not significantly dust obscured (§11.6). Moreover, it does not appear that the hosts of dark GRBs are brighter in the submillimeter as expected if the dust obscuration is global (Barnard et al. 2003). Finally, the localization of afterglows in the radio and X-rays allows the selection of host galaxies even if they are dusty. In particular, the only two GRBs in which significant obscuration of the optical afterglow has been inferred (GRB 970828: Djorgovski et al. 2001a; GRB 000210: Piro et al. 2002), have been localized thanks to accurate positions from the radio and X-ray afterglows, and have host galaxies with $R-K$ colors of 3.7 and 2.6 mag, not significantly redder than the general population of GRB hosts. Therefore, a bias against dust obscured host galaxies is not the reason for the bluer color of the sample.

An alternative explanation is that the distribution of dust in GRB hosts is different than in the radio pre-selected and submillimeter selected galaxies. This may be in terms of a spatially patchy distribution, which will allow more of the UV light to escape, or a different distribution of grain sizes (i.e., a different extinction law), possibly due to a different average metallicity. However, in both cases it is not clear why there should be a correlation between the dust properties of the galaxy and the occurence of a GRB.

Finally, it is possible that GRB host galaxies are preferentially in an earlier stage of the star formation (or starburst) process. In this case, a larger fraction of the shorter-lived massive stars would still be shining, and the overall color of the galaxy would be bluer relative to a galaxy with an older population of stars. One way to examine the age of the stellar population is to fit population synthesis models to the broad-band optical/NIR spectra of the host galaxies. This approach has recently been used by Chary et al. (2002) who find some evidence that the age of the stellar population in some GRB host galaxies (including the host of GRB 980703) is relatively young, of the order of $10-50$ Myr.

This result is also expected if GRBs arise from massive stars, as indicated by recent observations (e.g., Bloom et al. 2002b), since in this case GRBs would preferentially select galaxies with younger star formation episodes.

Regardless of the exact reason for the preferential selection of bluer galaxies relative to the radio pre-selected submillimeter population, two results seem clear: (i) The GRB host galaxies detected in the submillimeter and radio are likely drawn from a population that is generally missed in current submillimeter surveys, and (ii) GRB host galaxies may not be a completely bias-free sample.

The first point is particularly interesting in light of the fact that optical estimates of the SFR based on recombination and forbidden line luminosities do not identify them as particularly exceptional. Therefore, while similar galaxies are not necessarily missed in optical surveys, their star formation rates are likely under-estimated.

SECTION 11.8

Conclusions and Future Prospects

We presented the most comprehensive SCUBA, VLA, and ATCA observations of GRB host galaxies to date. The host galaxy of GRB 000418 is the only source detected with high significance in both the submillimeter and radio, while the host galaxy of GRB 000210 is detected with $S/N \approx 3.3$ in the submillimeter when we combine our observations with those of Barnard et al. (2003). When taken

in conjunction with the previous detections of GRB 980703 in the radio (Berger et al. 2001b) and GRB 010222 in the submillimeter (Frail et al. 2002), these observations point to a $\sim 20\%$ detection rate in the radio/submillimeter. This detection rate confirms predictions for the number of submillimeter bright GRB hosts, with $F_\nu(350\,\mathrm{GHz}) \sim 3$ mJy, based on current models of the star formation history assuming a large fraction of obscured star formation (Ramirez-Ruiz et al. 2002).

The host galaxies detected in the submillimeter and radio have star formation rates from about 200 to 700 $M_\odot$ yr^{-1}, while statistically the non-detected sources have an *average* SFR of about 100 $M_\odot$ yr^{-1}. These star formation rates exceed the values inferred from various optical estimates by over an order of magnitude, pointing to significant dust obscuration within the GRB host galaxies detected in the submillimeter and radio, and possibly the sample as a whole.

Still, the optical afterglows of the bursts that exploded in the submillimeter/radio bright host galaxies did not suffer significant extinction, indicating that: (i) the GRBs did not explode in regions where dust obscuration is significant, or (ii) the UV and X-ray emission from the afterglow destroys a significant amount of dust in the local vicinity of the burst.

We have also shown that GRB host galaxies, even those detected in the submillimeter/radio, have bluer $R-K$ colors compared to galaxies selected in the submillimeter or radio bands in the same redshift range. This is not the result of an observational bias against dusty galaxies in the GRB host sample since the afterglows of GRBs which exploded in the radio/submillimeter bright hosts were not significantly obscured. More likely, this is the result of younger stellar populations in these galaxies, or possibly a patchy dust distribution. If the reason is younger stellar population then this provides additional circumstantial evidence in favor of massive (and hence short-lived) stars as the likely progenitors of GRBs.

A potential bias of the GRB host galaxy sample is that the popular "collapsar" model of GRBs calls for high mass, low metallicity stellar progenitors (MacFadyen & Woosley 1999). This may result in preferential selection of low metallicity (and hence less dusty) host galaxies. However, it appears that GRB progenitors can even have solar metallicity, and that a very low metallicity is unfavored by the required initial conditions for a GRB explosion. Moreover, studies of the Milky Way, local galaxies (e.g Alard 2001), and high-z galaxies (e.g., Overzier et al. 2001), indicate that there are considerable variations in metallicity within galaxies. This may be especially true if several independent episodes of star formation have occured within the galaxy. Thus, even if there is a bias towards low metallicity for GRB progenitors (and hence their immediate environments) it is not obvious that this introduces a bias in the host galaxy sample.

Nonetheless, while the observations presented in this paper clearly indicate the potential of GRB selection of high-z galaxies for the study of star formation, a much larger sample is required to complement existing optical and submillimeter surveys. This may become possible in the near future with the upcoming launch (Sep. 2003) of SWIFT. With an anticipated rapid ($\sim$ 1 minute) and accurate localization of about 150 bursts per year, the GRB-selected sample will probably increase to several hundred galaxies over the next few years. The rapid localization would most likely result in a large fraction of redshift measurements thanks to the bright optical afterglows.

In addition to the localization of a large number of GRB hosts, the study of these galaxies (as well as those in other samples) would greatly benefit from the advent of new facilities, such as SIRTF, ALMA, EVLA, and the SKA. In Figure 11.7 we again plot the rest-frame SEDs of Arp 220 and the submillimeter/radio bright GRB hosts. Overplotted on these SEDs are the 1σ sensitivities of SIRTF, ALMA, and the EVLA for 200-sec exposures at redshifts 1 and 3, as well as the sensitivities of current instruments (VLA and SCUBA).

The contributions of these new facilities to star formation studies are threefold: (i) increased sensitivity, (ii) increased resolution, and (iii) increased frequency coverage. These improvements will serve to ameliorate the main limitations of present radio, submillimeter, and IR observations (§11.1), by allowing the detection of more representative star forming galaxies at high redshift, in addition to a better constraint on the total dust bolometric luminosity and accurate localizations, which would facilitate

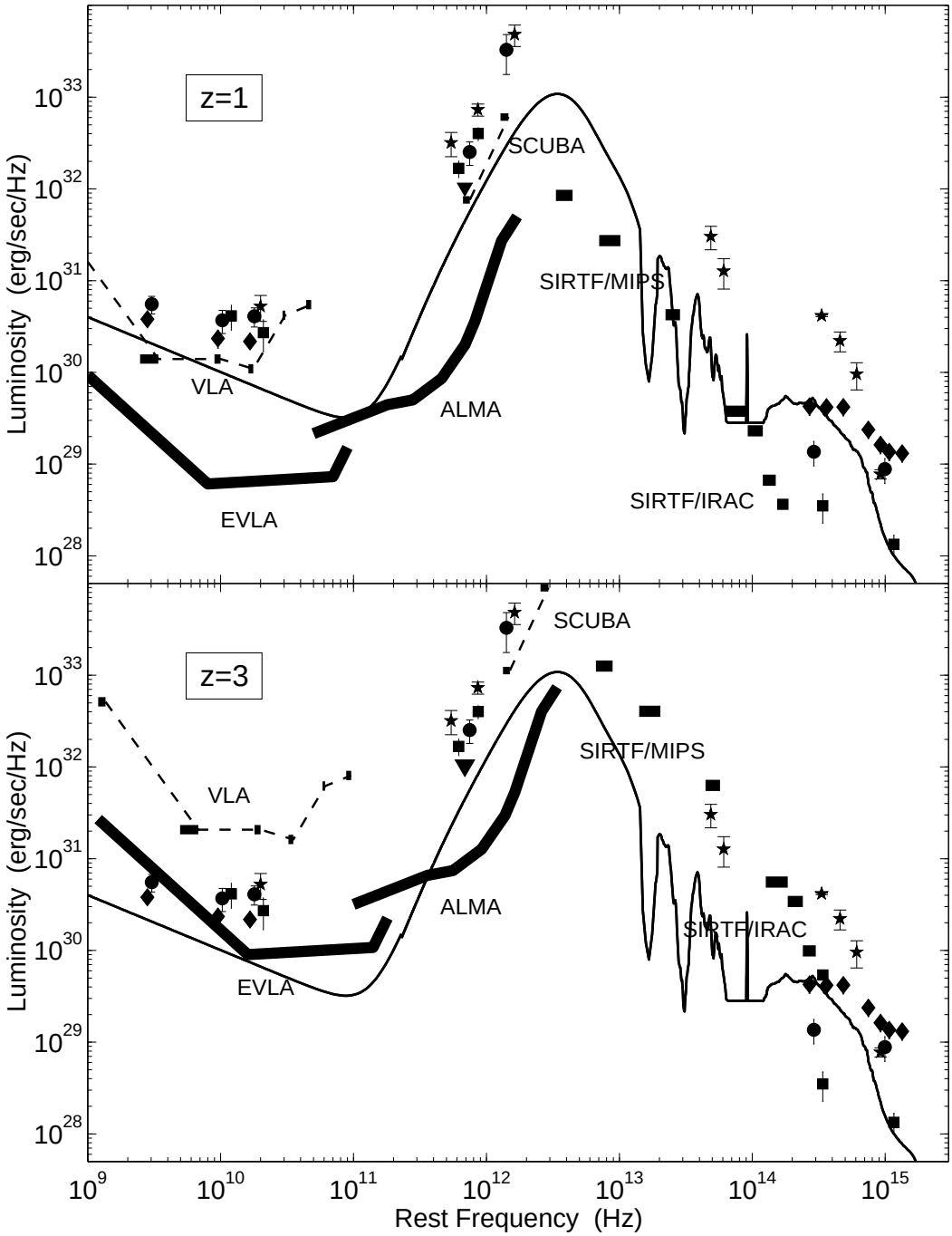

Figure 11.7: Same as Figure 11.3, overplotted with the EVLA, ALMA, and SIRTF bands at $z = 1$ and $z = 3$. The shaded regions correspond to the 1σ sensitivity in a 200 sec exposure for each instrument, while the dashed lines are the typical 1σ sensitivities for current instruments (i.e., VLA and SCUBA). Clearly, the new observatories will allow a significant increase in sensitivity, and spectral coverage over current instruments. As a result, the radio/submillimeter/IR observations will be able to probe lower luminosity (and hence more typical) star-forming galaxies.

follow-ups at optical wavelengths. In conjunction with increasingly larger samples of galaxies selected in the optical, the radio/submillimeter/IR, and by GRBs, the future of star formation studies is poised for great advances and new discoveries.

We thank A. Blain, A. Shapley, and the referee K. Adelberger, for helpful discussions and suggestions, and G. Moriarty-Schieven for help with the data reduction. We also thank S. Chapman for providing us with the optical/NIR colors and redshifts of radio pre-selected submillimeter galaxies prior to publication.

Table 11.1. Submillimeter Observations of GRB Host Galaxies

Source	z	Obs. Date (UT)	$F_\nu(350\,\mathrm{GHz})$ (mJy)	$F_\nu(670\,\mathrm{GHz})$ (mJy)	$\langle F_\nu(350\,\mathrm{GHz})\rangle$ (mJy)
GRB 970228	0.695	Nov. 1, 2001	-1.58 ± 1.34	-21.4 ± 18.6	
		Nov. 2, 2001	0.42 ± 1.61	-10.9 ± 21.4	-0.76 ± 1.03
GRB 970508	0.835	Sep. 9, 2001	-1.70 ± 1.56	-12.2 ± 48.4	
		Sep. 10, 2001	-0.53 ± 1.60	3.2 ± 64.8	
		Sep. 12, 2001	-3.64 ± 2.43	6.0 ± 34.2	-1.57 ± 1.01
GRB 971214	3.418	Nov. 2, 2001	0.49 ± 1.11	-14.2 ± 12.6	0.49 ± 1.11
GRB 980329	—	Sep. 13, 2001	1.22 ± 1.62	8.6 ± 10.2	
		Oct. 29, 2001	2.06 ± 0.99	-27.4 ± 21.6	1.83 ± 0.84
GRB 980613	1.096	Nov. 1, 2001	2.84 ± 1.87	92.6 ± 95.9	
		Nov. 2, 2001	2.21 ± 1.77	30.3 ± 64.4	
		Dec. 7, 2001	0.93 ± 1.33	22.6 ± 17.6	1.75 ± 0.92
GRB 980703	0.966	Sep. 10, 2001	-2.40 ± 1.30	-22.6 ± 18.6	
		Sep. 12, 2001	-0.84 ± 1.33	-13.9 ± 10.7	-1.64 ± 0.93
GRB 991208	0.706	Dec. 6, 2001	-2.65 ± 1.83	9.1 ± 26.9	
		Dec. 7, 2001	-0.08 ± 1.42	26.0 ± 17.2	-1.04 ± 1.12
GRB 991216	1.020	Oct. 31, 2001	0.09 ± 1.20	-6.5 ± 21.3	
		Nov. 3, 2001	1.23 ± 1.85	-30.2 ± 31.1	
		Nov. 4, 2001	0.73 ± 2.60	25.6 ± 128.5	0.47 ± 0.94
GRB 000210	0.846	Sep. 12, 2001	3.96 ± 2.27	98.1 ± 48.2	
		Sep. 13, 2001	4.34 ± 1.63	70.1 ± 45.1	
		Sep. 14, 2001	-0.01 ± 1.87	-6.4 ± 87.1	2.97 ± 0.88
GRB 000301C	2.034	Dec. 29, 2001	1.02 ± 1.99	21.4 ± 10.7	
		Dec. 30, 2001	-2.71 ± 1.79	-18.7 ± 25.1	-1.04 ± 1.33
GRB 000418	1.119	Oct. 30, 2001	3.80 ± 2.11	9.4 ± 56.7	
		Oct. 31, 2001	3.59 ± 1.35	65.1 ± 31.4	
		Nov. 1, 2001	2.32 ± 1.46	31.9 ± 26.1	3.15 ± 0.90
GRB 000911	1.058	Sep. 13, 2001	0.56 ± 1.69	4.7 ± 22.7	
		Sep. 14, 2001	-0.37 ± 2.68	-11.1 ± 41.2	
		Oct. 31, 2001	0.95 ± 2.25	-35.0 ± 66.2	
		Nov. 3, 2001	6.73 ± 2.08	56.5 ± 52.3	
		Nov. 4, 2001	3.07 ± 1.82	-49.0 ± 51.3	2.31 ± 0.91
GRB 011211	2.140	Dec. 29, 2001	1.64 ± 1.61	8.1 ± 15.2	
		Dec. 30, 2001	-0.11 ± 1.60	-14.3 ± 42.7	
		Dec. 31, 2001	3.88 ± 2.26	17.7 ± 68.0	1.39 ± 1.01

Note. — The columns are (left to right), (1) Source name, (2) source redshift, (3) UT date for each observation, (4) flux density at 350 GHz, (5) flux density at 670 GHz, and (6) weighted-average flux density at 350 GHz.

Table 11.2. Radio Observations of GRB Host Galaxies

Source	z	Telescope	Obs. Dates (UT)	Obs. Freq. (GHz)	F_ν (μJy)
GRB 970828	0.958	VLA	Jun. 4–7, 2001	8.46	12 ± 9
GRB 980329	—	VLA	Jul. 22 – Sep. 10, 2001	8.46	18 ± 8
GRB 980613	1.096	VLA	May 18–26, 2001	8.46	11 ± 12
GRB 981226	—	VLA	Jul. 24 – Oct. 15, 2001	8.46	21 ± 12
GRB 991208	0.706	VLA	Apr. 14 – Jul. 20, 2001	8.46	21 ± 9
GRB 991216	1.020	VLA	Jun. 8 – Jul. 13, 2001	8.46	11 ± 9
GRB 000210	0.846	VLA	Sep. 16 – Oct. 12, 2001	8.46	18 ± 9
GRB 000301C	2.034	VLA	Jun. 15 – Jul. 22, 2001	8.46	23 ± 7
GRB 000418	1.119	VLA	Jan. 14 – Feb. 27, 2002	1.43	69 ± 15
		VLA	Dec. 8, 2001 – Jan. 10, 2002	4.86	46 ± 13
		VLA	May 28 – Jun. 3, 2001	8.46	51 ± 12
GRB 000911	1.058	VLA	Mar. 21 – Apr. 2, 2001	8.46	6 ± 17
GRB 000926	2.037	VLA	Jun. 11 – Jul. 12, 2001	8.46	33 ± 9
GRB 010222	1.477	VLA	Sep. 29 – Oct. 13, 2001	4.86	19 ± 10
		VLA	Jun. 24 – Aug. 27, 2001	8.46	17 ± 6
GRB 990510	1.619	ATCA	Apr. 28, 2002	1.39	9 ± 35
GRB 990705	0.840	ATCA	Apr. 21–22, 2002	1.39	40 ± 34
GRB 000131	4.5	ATCA	Apr. 28, 2002	1.39	52 ± 32
GRB 000210	0.846	ATCA	Apr. 27–28, 2002	1.39	80 ± 52

Note. — The columns are (left to right), (1) Source name, (2) source redshift, (3) Telescope, (4) range of UT dates for each observation, (5) observing frequency, and (6) peak flux density at the position of each source.

Table 11.3. Star Formation Rates in GRB Host Galaxies Derived from Submillimeter and Radio Observations

Source	Submm SFR ($M_\odot$ yr^{-1})	Radio SFR ($M_\odot$ yr^{-1})	Optical SFR ($M_\odot$ yr^{-1})
GRB 970228	< 335	—	1
GRB 970508	< 380	—	1
GRB 970828	—	80 ± 60	1.2
GRB 971214	120 ± 275	—	3
GRB 980329[a]	460 ± 210	615 ± 275	—
GRB 980613	380 ± 200	50 ± 140	—
GRB 980703	< 380	180 ± 25	10
GRB 981226[b]	—	150 ± 85	—
GRB 990510	—	190 ± 750	—
GRB 990705	—	190 ± 165	—
GRB 991208	< 370	70 ± 30	20
GRB 991216	< 395	80 ± 70	—
GRB 000131	—	9800 ± 6070	—
GRB 000210	560 ± 165	90 ± 45	3
GRB 000301C	< 670	640 ± 270	—
GRB 000418	690 ± 195	330 ± 75	55
GRB 000911	495 ± 195	85 ± 70	2
GRB 000926	—	820 ± 340	—
GRB 010222	610 ± 100	300 ± 115	1.5
GRB 011211	350 ± 255	—	—

Note. — The columns are (left to right), (1) Source name, (2) SFR derived from the submillimeter flux, (3) SFR derived from the radio flux, and (4) SFR derived from various optical estimators. The upper limits represent 2σ values in the case when the measured flux was negative (see Table 11.1).